ALIGNED FIELDS, MAGNETO-FLUID DYNAMIC FLOW PAST BODIES

Thesis by

Gerold Yonas

In Partial Fulfillment of the Requirements

For the Degree of

Doctor of Philosophy

California Institute of Technology

Pasadena, California

1966

(Submitted May 9, 1966)

ACKNOWLEDGEMENTS

I would like to gratefully acknowledge the assistance of the following people: Dr. H. W. Liepmann, my thesis advisor, who together with Dr. T. Maxworthy guided my research, Dr. J. D. Cole for his interest in the theoretical problem, and all of the members of the Fluid Physics Section at the Jet Propulsion Laboratory, who provided me with many invaluable discussions.

I would like to thank the following people who assisted with the experiment: D. Griffith who operated and maintained the JPL Sodium Flow Facility, E. Coury who assisted with model fabrication and assembly, G. Hotz and G. Bastien for their help with design of the test apparatus, and K. MacDavid and C. Dunlap who assisted with strain gauge aspects. I would also like to thank Mrs. B. Paul who typed the final manuscript and its many revisions. I am grateful for the financial assistance of the Daniel and Florence Guggenheim Fellowship (1962-63), and the support provided by the Jet Propulsion Laboratory (1963-66) for this research as well as for myself.

Finally, my heartfelt thanks must go to my wife Jane, who has provided the encouragement and patience which was so necessary to the completion of this work.

Abstract

The drag of spheres and disks has been measured in a flow of liquid sodium with an aligned magnetic field. The experiments were carried out for $10^4 < Re < 25 \times 10^4$ and N, the interaction parameter, satisfying $0.1 < N < 80$. The sphere C_D was not a function of N for $N \lesssim 0.3$, began to increase appreciably for $N \backsim 1.0$, and reached an asymptotic dependence proportional to $\sqrt{N}$ for $N > 10$. The disk gave a C_D which was relatively unchanged for $N < 10$, began to increase for $N \backsim 10$, and had approximately the same value as for spheres for $N > 20$. We conclude, that for high N, flows are characterized by C_D insensitive to body shape and emphasize this range in our discussion. A physical model is presented which involves stagnant regions which grow in length as N increases, and are separated from the outer flow by thin dissipation layers. A singular perturbation technique is suggested for the theoretical treatment of such layers.

Table of Contents

Chapter		Page
I	Introduction	1
II	Description of Experiment	15
III	Analysis of Data	22
IV	Experimental Results	26
V	Discussion of Results	31
VI	Theoretical Discussion	37
VII	Conclusion	50
References		52
Figures		57

List of Symbols

$V_o \bar{e}_x$	velocity at infinity
$B_o \bar{e}_x$	magnetic field at infinity
P_o	pressure at infinity
σ	conductivity
ρ	density
μ	permeability
η	viscosity
ν	kinematic viscosity
d	body diameter
D	tunnel diameter
n	frequency of drag oscillations
A_o	tunnel area based on diameter D
A	tunnel area minus projected area of body
K	solid body blockage correction factor
$\bar{V} = \bar{V}'/V_o$	dimensionless velocity
$\bar{B} = \bar{B}'/B_o$	dimensionless magnetic field
$P = (P' - P_o)/\frac{1}{2} \rho V_o^2$	dimensionless pressure
$\bar{J} = \bar{J}' \mu d/B_o$	dimensionless current density
$H = P + V^2/2$	dimensionless Bernoulli function
$Rm = \sigma \mu V_o d$	magnetic Reynolds number
$Re = V_o d/\nu$	Reynolds number
$Pr_m = \sigma \mu \nu$	magnetic Prandtl number

$M = B_o\, d \sqrt{\sigma/\rho\nu}$	Hartmann number
$\alpha = B_o/V_o\sqrt{\rho\mu}$	Alfvén number
$L = \alpha\, Rm = B_o \sigma\, d \sqrt{\mu/\rho}$	Lundquist number
$N = \alpha^2 Rm = B_o^2 \sigma\, d/\rho\, V_o$	interaction parameter
$S = n\, d/V_o$	Strouhal number
$C_D = 8\ \text{drag}/\rho\, V_o^2\, d^2\pi$	drag coefficient
C_{D_o}	drag coefficient without field
C_{D_c}	drag coefficient corrected for blockage
Ω	angular velocity
$\tilde{x}$, $\tilde{y}$	dissipation layer coordinates
$\tilde{V}_x$, $\tilde{B}_x$, $\tilde{P}$	dissipation layer variables
$f(N)$	order of magnitude of layer thickness
$g(N)$	order of magnitude of layer pressure
$\gamma\,(Rm\ ,\ N)$	order of magnitude of field perturbation
$\lambda_{1,2}$	generalized Reynolds number used in linear theory (Gourdine)
$u_{1,2}$	perturbation velocity used in linear theory
ϵ	slenderness ratio used in thin airfoil theory

CHAPTER I

Introduction

Magneto-fluid dynamics (MFD) has been widely heralded in recent years as a subject of promise and worthy of great interest. Its marriage of the fundamental principles of electromagnetism and fluid mechanics has provided numerous authors with challenging new problems. Unfortunately, unless the work was motivated by actual engineering applications, its direction has generally been away from problems which are physically realizable. This is understandable because of the complexity of the exact equations which have forced various authors into using certain simplifying assumptions. Many of these assumptions are clearly non-physical, whereas others are meant to retain some of the characteristic features of certain flow regimes. One restricted problem, MFD flow over bodies, has been particularly popular as evidenced by an admittedly incomplete bibliography given by Sears and Resler (1) of some 71 articles. It is clear that in spite of their effort, few authors would have been willing to predict the outcome of any actual MFD measurement. This alone is sufficient reason for attempting such an experiment.

The experiment discussed here is concerned with the drag of bodies in a flow of liquid sodium with an applied magnetic field parallel to the free stream velocity. We will first discuss only that portion of the theoretical effort which deals with incompressible fluids and aligned fields. In practice, laboratory experiments would have to be done in

liquid metals and we will emphasize the material properties of such fluids in our discussion. We must first define the important parameters which appear in the steady dimensionless equations of motion:

$$\bar{V}\cdot\nabla\bar{V}+\nabla P = N(\bar{V}\times\bar{B})\times\bar{B}+\frac{1}{Re}\nabla^2\bar{V} \qquad (a)$$

$$\nabla\times\bar{B} = Rm\,(\bar{V}\times\bar{B}) \qquad (b) \qquad (1)$$

$$\nabla\cdot\bar{B} = \nabla\cdot\bar{V} = 0 \qquad (c)$$

where

$$\bar{V}=\frac{\bar{V}'}{V_o}\,, \quad P=\frac{P'-P_o}{\rho V_o^2}\,, \quad x=\frac{x'}{d}\,, \quad \bar{B}=\frac{\bar{B}'}{B_o}$$

the primed quantities being the physical variables. One can show from the Π theorem (2) that in addition to the force coefficient, we can choose three non-dimensional parameters which characterize the problem. The three found most convenient for our work are

$$N = \frac{B_o^2\sigma d}{\rho V_o} \quad , \text{ interaction parameter}$$

$$Re = \frac{V_o d}{\nu} \quad , \text{ Reynolds number} \qquad (2)$$

$$Rm = \sigma\mu V_o d \quad , \text{ magnetic Reynolds number}$$

N and 1/Re are, respectively, the ratio of magnetic and viscous forces to the inertial force. The physical interpretation of Rm

is not as clear due to the coupling between the momentum equation (1a) and the induction equation (1b). Childress (3) has pointed out that by making N arbitrarily large with Rm fixed, the relative importance of the induced field can be decreased. This is in contrast to the prevalent view of Rm alone defining the perturbation of the magnetic field.

Let us, at this point, further limit our discussion by considering only the case of aligned fields, i.e., problems in which the applied magnetic field is taken to be parallel to the velocity at infinity. Considerable interest has been shown in the more general problem of oblique fields (4, 5) or the crossed field case (6). Stewartson (7) considers the inviscid finite conductivity problem for oblique fields and shows that the aligned field case is not a continuous limit of the nonaligned problem due to a singular nature of the wake structure. We must therefore be careful in extending any conclusions from this special case to the more general one.

We are unable to discuss the relationship of the three parameters already noted unless we consider the coupling between (1a) and (1b). This is most easily done by linearizing the velocity and magnetic fields. Gourdine (8) has done this for the general steady problem of flow over a body, finding two rotational modes described by the equations

$$(\nabla^2 - \partial_{1,2}\frac{\partial}{\partial x})\, u_{1,2} = 0 \qquad \text{(a)} \qquad (3)$$

where

$$\partial_{1,2} = \tfrac{1}{2} Re \left[(1+Pr_m) \pm \sqrt{(1+Pr_m)^2 - 4Pr_m\left(1-\frac{N}{Rm}\right)} \right] \quad (b)$$

The ratio $Rm/Re = \sigma\mu\nu$ has been replaced by the symbol Prm termed the magnetic Prandtl number. This material property has the following values:

Sodium at 135°C.	$Prm = 10^{-5}$
Nak at 20°C.	$Prm = 10^{-6}$
Hg at 20°C.	$Prm = 10^{-6}$

The ratio N/Rm more commonly appears as $\alpha^2 = \frac{B_o^2}{\rho\mu V_o^2}$, the Alfvén number, and we can consider it as further classifying the types of flows. For $\alpha^2 >> 1$ (sub-Alfvénic), and $Prm << 1$

$$\partial_{1,2} \doteq \tfrac{1}{2} Re \left[1 \pm \sqrt{1+4\,\frac{N}{Re}} \right] \quad (4)$$

Again, we consider typical values which could be realized in an experiment:

B = 10,000 gauss, v = 50 cm/sec

Sodium at 135°C.	$N/Re = 10^{-2}$
Nak at 20°C.	$N/Re = 10^{-2}$
Hg at 20°C.	$N/Re = 10^{-4}$

We therefore write:

$$\alpha_{1,2} \doteq -N, Re \tag{5}$$

On the other hand, for $\alpha^2 \ll 1$ (super-Alfvénic):

$$\alpha_{1,2} \doteq \frac{1}{2} Re \left[1 + Pr_m \pm (1 - Pr_m) \right]$$

$$\alpha_{1,2} \doteq Re, Rm \tag{6}$$

we can then deduce the general character of the far field from Eq. (3a) for these two cases. This is shown in Fig. 1 (9). The super-Alfvénic flow has two wakes extending downstream, whereas the sub-Alfvénic case has a diffuse forward wake and an ordinary viscous wake downstream.

By considering physical parameters, we have eliminated the cases $N/Re \gg 1$ and $Prm \gg 1$. Few authors have treated

$Prm \gg 1$ problems, but the case $N/Re \gg 1$ has attracted a great deal of attention. Chester (10) and Chang (11) have solved the modified Stokes problem under the above restriction. Childress (12) emphasizes that the value of N/Re delineates the important cases. He considers the case $N/Re \gg 1$ in detail using an inner and outer expansion technique. He also includes a brief discussion of the more general case suggesting an outer expansion which is seen to depend on N only for $N/Re \ll 1$. Unfortunately, he does not discuss solutions of the outer problem for that case in this work, but only shows that this general limit is consistent with his conclusions for $N/Re \gg 1$. Chang's work contains essentially the same conclusions but utilizes several expansions in various regions of the flow. Although the last two papers discussed do not solve the physical problem, they do point the way to techniques which seem very promising.

Much emphasis has also been placed on flows of inviscid, perfect conductors. This rather singular case has proven to be the source of a great deal of controversy. Here the material property Prm is indeterminate and Stewartson (13) argues that $Prm \longrightarrow 0$ be taken as the proper limit in accordance with physical problems. If we consider sub-Alfvénic flows, then this describes the limit $N \longrightarrow \infty$, $Re \longrightarrow \infty$ in the linear problem already discussed. Both wakes shown in Fig. 1 collapse into the x-axis and the problem appears to have the inherent uniqueness difficulties as does the infinite Re case in ordinary viscous flows.

For this case, Stewartson (13, 14) finds that flows over bodies result in stagnant regions extending to infinity, whereas Sears and Resler (15) obtain a solution which involves irrotational fields outside of an infinitesimally thin "magnetic boundary layer" attached to the body. Stewartson (13), using a linear theory, and Ludford (16), by considering the manner in which Alfvén waves alter the flow field, treat an initial value problem and state that the Sears, Resler solution can not be set up from a state of rest. In addition, Stewartson (17) considers the magnetic boundary layer concept in detail showing that for sub-Alfvénic flows the boundary layer would have to include reversed flow at the leading edge. He suggests that a more likely consequence would be separation of the layer and formation of a forward wake. It would indeed be exciting to be able to resolve this controversy through experiments. We are, in fact, tempted to compare the sub-Alfvénic, large N results with the predictions for large Rm. The linear theory seems to point to this since Rm is no longer a parameter for very sub-Alfvénic flows, Eq. (5). Unfortunately, this is solely a consequence of the linearization, and such a comparison would be misleading.

In order to show this, we must consider the non-linear problem. This is best done by utilizing an equation derived by Tamada (18). He considers the inviscid momentum equation rewritten in terms of the dimensionless Bernoulli function $H = P + V^2/2$:

$$\nabla H + \bar{V} \times (\nabla \times \bar{V}) = \alpha^2 \bar{J} \times \bar{B}$$

Dotting both sides with $\bar{V}$, we get

$$\bar{V} \cdot \nabla H = -\alpha^2 \bar{J} \cdot (\bar{V} \times \bar{B}) \tag{7}$$

If $Rm = \infty$ and we require $\bar{V}$ parallel to $\bar{B}$ at infinity, then one can show from (1b) that

$$\bar{V} \times \bar{B} = 0$$

Hence

$$\bar{V} \cdot \nabla H = 0 \tag{8}$$

On the other hand, we can have $N \longrightarrow \infty$ with Rm finite by letting $\alpha^2 \to \infty$. Then

$$\bar{V} \cdot \nabla H = -\frac{\alpha^2}{Rm} J^2 \tag{9}$$

and H can decrease along streamlines in contrast to the result for $Rm = \infty$. If we consider the physical problem again, we get for $d = 1$ cm, $B_0 = 10{,}000$ gauss, $V_0 = 50$ cm/sec

Sodium at 135°C.	N = 100	Rm = 0.1	$\alpha^2 = 1000$
Nak at 20°C.	N = 100	Rm = 0.1	$\alpha^2 = 1000$
Hg at 20°C.	N = 1.0	Rm = 0.01	$\alpha^2 = 100$

We must conclude that for physical problems, large N flows are compatible only with $Rm \longrightarrow 0$, and experiments are incapable of shedding light on the sub-Alfvénic infinite conductivity problem.

Other authors have considered problems of greater physical interest, and also of much less mathematical complexity. Reitz and Foldy (19) consider the first-order perturbation to the pressure distribution by using the unperturbed potential velocity field and magnetic fields to calculate the current and the body force. They also show that drag found from integrating the pressure gives the same result as integrating the total joule dissipation. Leonard (20) considers the same approximation, but in addition treats the case of small interaction but arbitrary Rm by using a relaxation method. Under similar conditions, Seebass and Tamada (21) find an exact solution for the magnetic field by using an integral equation derived from a Green's function technique. Finally, we must note that Tamada (18), by considering a perturbation expansion for small N, predicted that a nondiffusive velocity disturbance would exist downstream of the body, and Leonard confirmed this in his work.

These small interaction approximations could describe flows in which boundary layer separation plays no role; however, one certainly could not expect that such solutions would be of any relevance to high Re flows over bluff bodies. On the other hand, one could use such a technique to describe flows about semi-infinite bodies. Ahlstrom (22)has investigated the magnetic field distribution upstream of a

Rankine body moving through a tank of mercury. He utilizes such small interaction assumptions to predict the decay rate of the magnetic field in an unbounded fluid. He finds, however, that the shielding effect of the field coil on the moving field disturbance is dominant but is able to take this into account by considering an effective boundary value problem. One other experiment has been carried out that falls into this class. Motz (23) has measured the drag of an oscillating sphere immersed in mercury in an aligned field. There too, the zero order problem (no field) is describable by an inviscid flow field. He uses a theoretical explanation identical to that employed by Reitz and Foldy and finds excellent experimental correlation with those predictions.

In the above discussions, the operator $\bar{V}\cdot\nabla$ in the equations of motion is replaced by $\bar{V}_o\cdot\nabla$, where $\bar{V}_o$ is given by the potential velocity field. In this way a simpler linear problem is obtained. Another approximation is that of Oseen, $\bar{V}\cdot\nabla$ and $\bar{B}\cdot\nabla$ replaced by $\frac{\partial}{\partial x}$. This is done for arbitrary values of the parameters in discussing the wake behavior as Gourdine (8) does. Another view is to consider a thin airfoil theory which permits one to obtain a uniformly valid approximation throughout the entire flow field. This technique is used by Lary (24) for inviscid flows, who finds limits on the validity of such an approximation. He finds for $\alpha^2 >> 1$, Rm finite, two-dimensional problems:

$$C_D \sim \epsilon^2 N \qquad \text{for} \qquad N < 1$$

$$C_D \sim \epsilon^2 \sqrt{N} \qquad \text{for} \quad \frac{1}{\epsilon} < N < \frac{1}{\epsilon^2}$$

where ϵ is the slenderness ratio of the body. He attempts, however, to extend his results to the case $N >> \frac{1}{\epsilon^2}$ by using the magnetic boundary layer concept developed by Sears and Resler (15). The resulting no-slip condition on the magnetic field may be a consistent model for steady infinite Rm flows, but it certainly can play no role where diffusion of the magnetic field is present. As we saw earlier, the analogy between infinite Rm and infinite N flows was a misleading consequence of the linearization, and that the infinite conductivity approximation can have no physical relevance.

In an attempt to resolve the infinite conductivity problem, Stewartson (7) extends the inviscid thin airfoil approximation for fluids of finite conductivity by considering three separate problems. He first considers a linear problem similar to Lary's, but unsteady. He then takes the limit of the non-aligned problem as the angle between the velocity and magnetic fields tend to zero. There is general agreement on the character of the flow field and the predicted drag if N and the slenderness ratio are limited as Lary described. Stewartson emphasizes the restrictions on this linear theory and points out that a different point of view is required for very sub-Alfvenic flows with finite Rm , i.e., N becoming arbitrarily large. The third problem

he considers, the "strong field case," is not completely resolved though. He suggests that stagnant regions exist in this case, but he does not answer how one is to match such a near field to a far field approximation which is uniformly valid at infinity.

We have seen that consideration of the non-linear aspects of MFD problems have led in many cases to conclusions entirely different from those of the linear versions of the same problems. We can see from Eq. (9) that any linear theory will satisfy Eq. (8) since J is a perturbation quantity, and the change of the Bernoulli function is totally lost. The principal consequence of this, as pointed out by Tamada (18), is that the Oseen approximation misses the existence of the downstream vortical disturbance for inviscid flows. By considering the non-linear inviscid problem, Childress (3) concludes that general solutions are not necessarily continuous at infinity. He too admits the possibility of a "stationary wake" or a non-diffusive vortical region allowing finite velocity disturbances to reach to infinity downstream. The action of a small viscosity will be to diffuse this velocity perturbation leading to continuous behavior at infinity.

The problem then appears to involve a consideration of a non-linear near field and the matching to the proper far field which includes both joule and viscous dissipation. This theoretical problem is seen to coincide with the experimental restrictions which have already been delineated:

$$Re \gg 1 \ , \quad N/Re \ll 1 \ , \quad Prm \ll 1 \ , \quad \text{and} \quad (10)$$

$$Rm \ , \quad N \ \text{arbitrary.}$$

If in addition $N \gg 1$, $Rm \ll 1$, then we could expect that magnetic forces are dominant near the body and an inviscid analysis could be attempted for the near field. The difficulty of the problem is apparent and one would like to have some experimental knowledge that at least the description of the problem is correct. It was hoped that a measurement of the drag would tell us which parameters were important and what ranges of those parameters were critical.

Liepmann pointed out the importance of such an experiment, and attempts to measure MFD drag on bodies by timing the rise of buoyant spheres in the GALCIT mercury tow tank were begun in 1960 (2). These experiments proved to be unsuccessful and a technique using a sting mounted drag balance was started simultaneously with our work (25). Maxworthy, utilizing the terminal velocities of spheres falling through a column of sodium in an aligned field, noted a marked increase in drag for strong fields (26). The parametric range agreed with conditions (10) , but was limited to $N < 3.7$. He states that the drag coefficient scales with N/Re only. Private communications with him since then indicated that those results should be viewed with skepticism due to difficulties involved with the experiment. Upon his suggestion, measurements of the drag of bodies were carried out using the JPL Sodium Flow Facility (27). There were definite advantages over

the previous techniques:

a) The field boundary conditions encountered in an unsteady experiment would not exist.

b) Conventional drag balance techniques could be used.

c) High values of N and Re could be obtained.

In the following chapters we will discuss the experiment and its results. We will present, in Chapter VI, a theoretical model motivated by the experiment, but a complete analytical treatment will not be attempted. We will, however, suggest the proper description of the physical problem and one possible way of solving it.

CHAPTER II

Description of Experiment

The liquid sodium flow facility at the Jet Propulsion Laboratory, shown schematically in Fig. 2 (27), was designed to function as a basic research tool in magneto-fluid dynamics, its role being similar to that of the wind tunnel in ordinary fluid dynamics. Although much engineering interest has been stimulated in cross-field flows, we have seen the considerable amount of theoretical efforts contributed to the aligned field case. In particular, it was desirable to create flows in which the interaction parameter could be made much larger than one. Because of its high conductivity and low density, sodium seemed ideal for this purpose, but as Cowling (28) points out, "no liquid can be regarded as such when it forces an experimenter to wear asbestos clothing when approaching his apparatus."

Not withstanding the difficulties involved with handling the fluid, the next most important concern is to really achieve a situation simulating aligned fields. Due to the physical constraints on the length of the test section and magnet, end effects are of concern. At the ends of the magnet, the fringing field interacts with the flow, giving currents which can be convected to the central portion of the test section. In an attempt to minimize the currents generated at the entrance to the test section, an entrance nozzle which approximates the shape of the field was employed. Although this proved to be quite successful,

no such attempt was made to minimize the disturbances created at the exit. As a result large disturbances were created there and under the most severe conditions did reach the central portion of the test section.

It was therefore necessary to measure the velocity at the same location as that of the drag measurements. In order to do this, the stagnation pressure was measured in the entrance nozzle, and the static pressure was measured using a conventional static pressure probe. The results of these measurements at several field strengths are shown in Fig. 3. An extensive experimental investigation of this "exit effect" has been carried out by Maxworthy (29). He discusses there the suitability of the Pitot tube in such flows and limitations on the usefulness of this flow facility. He concludes that the velocity distribution is sufficiently uniform over the central half of the test section diameter to study flows over bodies under the most severe conditions that we can presently achieve. It is clear though that measurements at stronger fields than now presently employed would necessitate the use of either a longer test section or a shaped nozzle to minimize the interaction at the exit.

We can see from Fig. 3 that the centerline velocity without field is not a linear function of the flow meter output voltage. An integration of the velocity profiles shows that the flow meter voltage is indeed a non-linear function of the flow rate below 6 mv. The flow meter is of the standard circular, transverse-field type manufactured

by the MSA Research Corporation, and such a meter is generally considered to be linear in its behavior. This is true only if the velocity profile is axially symmetric, and the field uniform. Shercliff (30) discusses this matter and emphasizes that difficulties can occur in liquid metals for low flow rates. We have already discussed the importance of the interaction parameter and expect that for $N>1$ the velocity profile can be altered by the field with a resulting loss of the axial symmetry. In fact, N, based on the flow meter diameter, has a value of 5 for an output voltage of about 6 mv and it is not surprising that it has non-linear behavior for lower flow rates.

The magnet was designed so as to maximize the length over which the interior field was uniform. The actual distribution was measured using a RFL Hall effect gaussmeter. The field was found to be uniform over the central 70% of its length to within 3%. A calibration of the magnetic field at the body location, as a function of the power supply shunt voltage, was carried out using a Bell model 240 incremental gaussmeter. The Hall element used with this instrument was calibrated using a standard reference magnet giving an accuracy of $\pm$ 1%. This was not done with flow and one might consider the possibility of the field being perturbed due to currents propagating upstream from the exit. From the pressure distribution measurements, Maxworthy (29) has estimated the field perturbation due to the exit effect and states that it would be less than 1%.

Two magnet power supplies were used: A. O. Smith Company rectifier power supply, 1100-2500 Amps, $\leq$ 8% ripple peak-to-peak; Cristie Electric Corporation rectifier power supply, 0-1000 Amps, $\leq$ 1% ripple peak-to-peak. Fortunately, the ripple in both cases occurred at 360 cps which results in a skin depth in aluminum of $\sim$ .3 cm. Since the test section wall is $\sim$.5 cm thick, we can safely assume that the magnetic field was steady at the body location.

A strain gauge balance was chosen for the drag measurement due to its simplicity, small size, and high temperature capability. A full strain gauge bridge was attached to an aluminum beam located in a chamber adjacent to the test section wall (see Figs. 4 and 5). A wire suspension system was chosen so as to minimize support drag and interference effects. The bodies were suspended from three tungsten-rhenium wires attached to three identical beams and pre-set at an angle that maximized the sensitivity. The wires pass from the interior of the test section into the gauge chamber through 1/16" holes. The chamber was packed with a silicone grease, Dow Corning 11, to damp beam oscillations and to prevent sodium from reaching the gauges. No other protection was provided for the gauges, but all solder joints in the chamber were encapsulated in silicone rubber. The strain gauge bridge input voltage was provided by a Dynamics Corporation, Model 6313, bridge supply, and the steady component of the drag was measured on a Keithly model #149 milli-microvoltmeter.

The drag balance also served as an indication of the unsteadiness of the flow, although it was by no means intended to provide quantitative information of that kind. The unsteady component was amplified using a Dynamics Model 6496 differential D. C. amplifier and recorded on a Honneywell Visicorder oscillograph.

The drag balance test section was fabricated in two halves to allow for easy installation of various bodies and to permit calibration before and after each run. The upper half of the test section is shown in Fig. 6 attached to the balance used for calibration. The accuracy of the balance was $\pm$ .1 gram and the full scale of 1600 grams (force) was utilized. Although the strain gauges were mounted on a thin strip of aluminum within close proximity of each other providing excellent temperature compensation, the drag balance itself was still quite temperature sensitive. This was due to the lengthening of the wire and slight changes in the gauge factors of the strain gauges. It was therefore necessary to carry out the calibration at the operating temperature of 135^{o}C. The temperature of the gauges was measured using a chromel-alumel thermocouple embedded in the beam. During the calibration, the test section was filled with Dow Corning 200 fluid, wrapped with an electrical-heating tape and insulated. It was necessary to heat, then cool, the test section many times prior to calibration to remove air bubbles trapped in the grease. On cooling, the volume which had been occupied by the air was filled with the silicone fluid. If this

were not done, the gas bubbles adjacent to the beams would expand or contract with changes in test section static pressure. Some difficulties that arose for small loads, less than 10 grams, were attributable to this effect.

The two types of models used in this experiment, disks and spheres, were made from either non-magnetic stainless steel or brass. Tungsten-rhenium wire was employed for its high tensile strength and improved ductility over ordinary tungsten wire. Difficulties in supporting bodies arose due to fracture under fatigue, particularly at any edges over which the wire passed. In the final configurations, shown in Fig. 7, we see that all sharp bends are contained within the bodies and that the wires are constrained between two surfaces as they pass from the body.

Data was taken by pre-setting the magnet current and varying the pump speed. With the field on, all zeros were set and the flow rate was increased in regular increments. The following quantities were measured for each data point:

1. bridge output voltage;
2. strain-gauge beam temperature;
3. magnet power supply current;
4. flow-meter output voltage.

A selector switch was used to choose between these inputs which were all measured with the milli-microvoltmeter.

A separate apparatus was employed to study possible interference of the bodies on the tunnel boundary layer. The Reynolds number based

on the length from the start of the test section, Re_L , ranged between 140×10^3 and $3{,}500 \times 10^3$. The laminar wall boundary layer which would exist at least at the lowest velocities employed might have separated due to a small region of adverse pressure gradient created by the presence of the sphere (31). In order to investigate this possibility, an air flow visualization experiment was set up using an entrance nozzle previously employed in another experiment (32). An appropriately scaled test section made of plexiglass was used, and the velocity of flow was measured with a Pitot tube and a Betz manometer. Two visualization techniques were employed, oil injected into the boundary layer and cotton tufts attached to the suspension wires, neither of which gave any evidence of separation. We concluded that the tunnel boundary layer remained attached for $Re_L > 100{,}000$.

CHAPTER III

Analysis of Data

The following configurations were utilized:

Run #1	.250-in. sphere	- .005-in. support wires
Run #2	.500-in. sphere	- .010-in. support wires
Run #3	.750-in. sphere	- .010-in. support wires
Run #4	.500-in. sphere	- .005-in. support wires
Run #5	.500-in. disk	- .010-in. support wires.

In each case the drag balance was calibrated before and after each run to ensure reliable results. A typical calibration curve is shown in Fig. (8). For this particular run the balance was linear for loads less than 300 grams. The extent of the linear range varied greatly for different runs, being extremely sensitive to the initial angle of the suspension wires. The linear behavior existed generally only over a small portion of the total range of values measured, and most of the measurements had to be converted to drag in grams using such a curve. The calibration and interpolation could be carried out with an accuracy of $\pm$ 1%.

Raw data for the .750-in. sphere is shown in Fig. (9). Smooth curves were drawn through the data points, and the values used in the final computation were taken from these curves at flow rates denoted by the dashed lines. This facilitated computation and reduced the scatter for a particular field strength. There was some latitude in

drawing these curves, and we can attribute an accuracy of $\pm$ 2% at best to this technique.

The effect of strong fields on the centerline velocity has already been noted. The results of the velocity measurement were shown in Fig. (3). We see there that the largest magnet current, 2500 amps or 7050 gauss, has a measurable effect over the entire velocity range, whereas currents less than 1500 amps, 4260 gauss, do not affect the velocity for flow meter voltages greater than 1 millivolt. For each combination of magnet current and flow meter voltage, we find a free-stream velocity either from these curves or by interpolating for other fields. Inaccuracy in this separate measurement, curve fitting, and interpolation contribute an inaccuracy which can be estimated as $\pm$ 2%.

The material properties for sodium at the operating temperature of 135°C were found by interpolation from data appearing in the Liquid Metals Handbook (33). They are

$$\rho = .918 \times 10^{3} \quad \text{kg/m}^3$$
$$\sigma = .911 \times 10^{7} \quad \text{mho/meter}$$
$$\eta = .575 \times 10^{-3} \quad \text{kg/meter second.}$$

Although the temperature of the entire facility is regulated, records of the test section temperature show a variation between 132°C and 138°C. This results in an additional inaccuracy in ρ of $\pm$ .1% , in σ of $\pm$ 1% , and in η of $\pm$ 2% .

In calculating the sphere drag we must subtract the wire drag from the total force measured. We assumed that the wire drag coefficient was not affected by the field and used values for this quantity given in Schlichting (31). This assumption will be discussed later. The entire length of the suspension wires was used in this calculation with no allowance made for the test section wall boundary layer. On the other hand, the free stream velocity was used in this calculation which does not take into effect the accelerated flow near the body or the blockage effect.

Fortunately, this uncertainty is relatively unimportant in most of the measurements because the wire drag itself is only a small percentage of the total drag. This is true because the ratio of the projected area of the wires to that of the sphere for Runs #1-4 are, respectively, .25, .10, .05, and .05. We see that the greatest difficulty arises for Run #1, and we expect that inaccuracies in estimating the wire drag will appear most strongly there. If we estimate an inaccuracy of $\pm$ 5% in the wire drag calculation, the resulting inaccuracy in the calculated drag coefficient will be, respectively, $\pm$ 2.5%, 1%, .5%, and .5% for Runs #1-4 for the no-field case. As the field strength is increased, the wire drag becomes a smaller percentage of the total, and this inaccuracy becomes unimportant.

The calibration of the magnet as a function of the power supply shunt voltage was carried out with an accuracy of $\pm$ 1%. However, due to the changing temperature of the magnet and drift of the power supply

itself during a run at a given current setting, we must attribute an inaccuracy of $\pm$ 2% to the value of magnet field used in the calculation.

Without field the resulting maximum inaccuracy in the calculated drag coefficient is, respectively, $\pm$ 9.5%, $\pm$ 8%, $\pm$ 7.5%, and $\pm$ 7.5% for Runs 1-4. For strong fields the inaccuracy in wire drag becomes negligible and this estimate becomes $\pm$ 7% for all runs. We will see later that the only other important nondimensional parameter is N, and we estimate its maximum inaccuracy as $\pm$ 3.5%.

CHAPTER IV

Experimental Results

The drag coefficient, C_D, is plotted in Figs. 10, 11, 12 as a function of Re for Runs 1-3. The ranges of parameters can be summarized:

$$10{,}000 < Re < 250{,}000$$

$$0 < M < 1660$$

The range of Re is that which is characterized, for no field, by a laminar sphere boundary layer, separation upstream of the center of the sphere, and C_D relatively insensitive to Re. For a fixed Re the C_D increases monotonically with field, and for a fixed M it decreases monotonically with Re. Any exceptions to this are attributed to experimental scatter.

In Figs. 13, 14, 15 we see C_D plotted as a function of the interaction parameter N for various values of the Hartmann number M. The range here is

$$0 < N < 80$$

The correlation with the parameter, $N = \frac{B_o^2 \sigma d}{\rho V_o}$, can not be completely checked except by carrying out experiments in different fluids. In each run we only vary B_o and V_o and we see that C_D behaves like a function of B_o^2/V_o. The results of these runs are summarized in Fig. (16) where we show smooth curves fitted to the data shown in Figs. 13, 14, 15. We see that d/D, where D is the test

section diameter, remains as an independent parameter.

For $N \gtrsim 10$ the dependence of C_D is seen to be proportional to $N^{\frac{1}{2}}$ and for $N \lesssim .3$ it is independent of N. In both of these ranges we can estimate the blockage correction using a straightforward technique and compare it with the results shown in Fig. (17). There we see C_D plotted as a function of d/D for $N = 0$ and $N \gtrsim 10$. The experimental scatter, shown by the horizontal bars, is approximately that predicted in Chapter III. Smooth curves are drawn and an extrapolation is made to $d/D = 0$.

We assume that the blockage constraint has the simple effect of increasing the velocity that should be used in calculating the appropriate nondimensional parameters. Maskell (34) and others have discussed a blockage correction for bluff bodies, but this author was unable to find any experimental or theoretical results for spheres. For flows about bodies with a sharp edge, the separation point is fixed; however, it is possible that the blockage might have the additional effect of shifting the point of separation on a sphere. We attempt, nevertheless, to use a blockage correction based simply on the solid body blockage constraint:

$$V_o/V = A/A_o = (1 - d^2/D^2) = K$$

For the no-field case the extrapolated value is found to be $C_D = .40$, and for $N > 10$ it is given by $C_D/\sqrt{N} = .33$. This then yields

$$C_D = .40\ K^{-2} \quad ; \quad N = 0$$

and

$$C_D = .33\ \sqrt{N}\ K^{-3/2} \quad ; \quad N > 10$$

The following table gives the results of applying such a correction:

d/D	K^2	$K^{3/2}$	C_D N = 0	$C_D/\sqrt{N}$ N > 10	$K^2\ C_D/.40$ N = 0	$K^{3/2}C_D/.33\ \sqrt{N}$ N > 10
0	1.00	1.00	.40	.33	1.00	1.00
.125	.968	.977	.42	.34	1.02	1.01
.250	.878	.906	.45	.38	.988	1.04
.375	.738	.795	.49	.43	.904	1.04

The correction is seen to be well within the scatter for $N > 10$ but seems to overestimate the blockage correction for $N = 0$, $L/D = .375$.

For $N < 10$ neither C_D nor $C_D - 1$ obeys any simple power law with N. It was found that although no simple blockage correction could be applied, C_D/C_{D_o}, where C_{D_o} is the drag coefficient without field, is independent of d/D. This is shown in Fig. (18).

As we have seen, the sphere drag coefficient is relatively unchanged for $N < 1$. In reducing the data we assume that the wire drag has similar behavior, and since $N \lesssim 1.0$, based on the wire diameter of .010-in., we have strong support that this is a good approximation. In addition, Run #4 was specifically carried out to check this. The drag coefficient for the .500-in. sphere was remeasured using .005-in. support

wires. The results of this measurement are shown in Fig. (19), superimposed on those for Run #2.

In order to investigate the effect of body shape, the drag of a .500-in. disk with .010-in. suspension wires was measured. C_D vs Re for Run #5 is shown in Fig. (20). We see that the simple monotonic behavior which was characteristic of sphere drag does not appear here. At high Re , C_D is in fact lower with a field applied than without. In order to clarify this, we must again consider the effect of the blockage constraint.

Fortunately, considerable experimental and theoretical work has been carried out concerning the problem of blockage effect on disks. Maskell (34) points out that solid body blockage alone is insufficient to explain measured drag coefficients. With no blockage the disk wake is roughly twice as wide as the disk itself, and wake blockage must be taken into account. He establishes a model which is partly based on empirical evidence since no complete theory for bluff-body wakes exists. He presents a formula which is supported by the experiments of Fail, Lawford, and Eyre (35).

$$C_{D_c} = C_D/(1 + 2.5\ C_D\ d^2/D^2)$$

where C_D is the measured value and C_{D_c} the corrected value. The effect of this correction applied to the $M = 0$ result is shown in Fig. (21) along with the behavior of C_D as a function of N . We see that

although C_D drops below the no-field value in the range $1 < N < 10$, it rises again for $N < 1$. Within the accuracy of the experiment, it never drops below the corrected value.

Figure (21) also shows a comparison with the results for the .500-in. sphere. We see that for $N > 20$ there is good agreement between the two, and the asymptotic behavior of $\sqrt{N}$ is again reached.

The drag balance is sensitive to both unsteady lift and drag. Its response to an unsteady force is dependent on not only the frequency range, but also the steady force. Quantitative results would necessitate a difficult calibration procedure and at least one additional gauged beam. Hopefully, by measuring unsteady force at locations 120° apart, one could separate the lift and drag. This was not attempted, and oscillograph traces of the unsteady force were used only to give a rough idea of the dominant frequencies.

The traces demonstrated the existence of unsteadiness under certain conditions, and one could define the approximate range of the Strouhal number, $S = nd/V_o$, that appeared. Without field S was approximately .20 and it was clear that marked changes could occur even for weak fields. Fields of about 0.30 web/m^2 appeared to give steady drag over the full velocity range. Unsteadiness was apparent again for fields of approximately 0.50 web/m^2 and the frequencies decreased as the field was further increased. The Strouhal number of these strong field oscillations was quite small and dropped from a value of approximately .09 at 0.50 web/m^2 to .03 at 0.70 web/m^2.

CHAPTER V

Discussion of Results

The results of these measurements as illustrated in Figs. (17), (18), and (21) can be summarized here:

sphere drag

(i) $C_D \doteq .40\ (1 - d^2/D^2)^{-\frac{1}{2}}$ $\quad N = 0$

(ii) $C_D \doteq .33\ \sqrt{N}\ \ (1 - d^2/D^2)^{-3/2}$ $\quad N > 10$

(iii) $C_D \doteq C_{D_o}\ \ F(N)$ $\quad 0 < N < 10$

where $F(N)$ is relatively unchanged from $F(N = 0)$ for $0 < N < 1$, and approaches the behavior $\sqrt{N}$ as N approaches the value 10.

disk drag

(iv) $C_D \doteq .11\ (1 - 2.8\ \ d^2/D^2)^{-1}$ $\quad N = 0$

(v) $C_D \doteq .33\ \sqrt{N}\ \ (1 - d^2/D^2)^{-3/2}$ $\quad N > 20$

(vi) $C_D \doteq G(N)$ $\quad 0 < N < 20$

where $G(N)$ is relatively unchanged from $G(N = 0)$ for $0 < N < 1$, decreases to the value ~ 1.10 for $1 < N < 10$, and approaches the behavior $\sqrt{N}$ as N approaches 20.

We must first compare the measured sphere C_D for $N = 0$ with results quoted by others. Although we have loosely described the drag coefficient as being constant in the range $10{,}000 < Re < 250{,}000$,

previous empirical evidence does in fact show a systematic variation. Schlichting (31) exhibits a compilation of the work of various experimenters clearly showing this. One can see there that C_D increases from .39 to .48, then decreases to .40 as Re increases from 10,000 to 250,000. Due to the scatter in our zero field data, no such systematic variation can be observed. The extrapolated value of $C_D = .40$ for $d/D = 0$ should be compared with the range of C_D that exists for the same Re range. The accuracy attributed to our value is $\pm$ 8% so the range of C_D found here is .43 - .37, and overlaps the previous experimental evidence.

We have already pointed out that the solid body blockage correction seems to overestimate the increase in drag for $d/D = .375$ with no field. It is possible that movement of the separation point downstream is responsible for this effect. If this exists, it is also possible that the extrapolation to $d/D = 0$ does not properly take it into account. It is beyond the scope of this experiment, or for that matter, its intention to investigate this effect more fully. We are primarily interested in the strong field case, $N > 10$, and we noted that the solid body correction factor adequately described the behavior of C_D as a function of d/D. We can therefore surmise that the field acts both to fix the point of separation and to constrain the wake. We conclude from this that the boundary only increases the effective free stream velocity which must be used in calculating the proper nondimensional parameters.

For $N < 10$ we saw that C_D/C_{D_o} was only a function of N, d/D being eliminated by this normalization. Additionally, the critical value

of N at which C_D/C_{D_o} began to increase appreciably was 1, and the value of N at which the final behavior of $\sqrt{N}$ was reached is given approximately by 10. N is thus seen to delineate various flow regimes, which we might describe as follows:

$$N/Re \ll 1$$

$N < 1$, $Rm \backsim 1$: Separation of laminar viscous boundary layer dominates. Field has little effect.

$1 < N < 10$, $Rm \lesssim 1$: Intermediate range where separation of viscous boundary layer and MFD forces both play a role.

$N > 10$, $Rm \ll 1$: MFD forces dominate. Asymptotic high N behavior is reached.

We have shown that N/Re was also an important parameter in our discussion of the theory. We must emphasize that $N/Re < 10^{-2}$ throughout this experiment so that the asymptotic behavior $N > 10$ must include the restriction $N/Re \ll 1$. We expect that N/Re would again enter if we continued to increase N, holding Re fixed, so that N/Re exceeded 1. As already mentioned, this is not possible using conventional field strengths, $B_o \backsim 1$ web/m^2. In the laboratory these high values of N are achieved by reducing the free stream velocity, and as a result we are also restricted to $Rm \ll 1$.

We argued that the wire C_D had similar behavior with N as that of the sphere. Since $N_{wire} < 1.0$ we assumed that C_D is given by its zero field value and had no interference effect on sphere drag. This was also supported by experimental results shown in Fig. (19). Such wire supports have been investigated by others, and it is known that as long as the flow is subcritical (laminar boundary layer separation on upstream side of sphere), the wires have little effect (36). Such a support does, however, have a marked effect for the supercritical range which is never reached here. We conclude that the wire interference is negligible without field as long as the separation point is upstream of the point of attachment of the wires, and with field and $N > 1$ the magnetic field dominates the sphere wake behavior and drag coefficient.

The disk drag coefficient was shown to be adequately corrected for zero field from $C_D = 1.35 \pm .15$ to $1.10 \pm .10$. This shows good agreement with the value given by Fail, Lawford, and Eyre (35) of 1.12. For $N < 1$ the disk drag coefficient is little affected, and as before, $1 < N < 10$ appears to be an intermediate range. Although the separation point is fixed, the blockage effect leads to an additional complication. For $1 < N < 10$ C_D is actually lower than the value for $N = 0$, but it does not fall below the corrected value within the accuracy of the experiment. The magnetic field in this intermediate range has the apparent effect of eliminating the blockage constraint. We must emphasize, however, that we do not expect that the physical situation is a simple one. One can conclude that more detailed measurements of the flow and magnetic fields are required before we could hope to understand any such range

where two or more different effects are important.

For $N > 10$ the disk C_D is very close to that of the sphere and appears to reach the same asymptotic dependence for $N > 20$. This strongly implies that for $N > 10$ the flow field is relatively insensitive to the shape of the body.

We have already stated that insufficient evidence was obtained to draw quantitative conclusions concerning wake stability. There were indications though that weak fields were able to completely damp the dominant frequencies that existed without an applied field. This is consistent with the physical concept of the field providing a strong restoring force for oscillations normal to it. Similar results were obtained by Maxworthy (26) who noted non-oscillatory wake behavior for $N \backsim .5$. In addition, the suppression of turbulence due to an aligned field was noted by Globe (37) using a pipe flow of mercury in an aligned field. In this light, the reappearance of unsteadiness at much lower frequencies for strong fields is somewhat surprising. These low frequency oscillations appeared when the steady drag and presumably the flow configuration were considerably different from that with no field. It is possible that the wake was able to selectively amplify long wavelength disturbances which existed in the flow.

Wake measurements of the fluctuating field or velocity would be required in order to understand this result. The trend toward lower Strouhal numbers with increasing field seemed clear, although there seemed to be no dependence on N itself. On the contrary, C_D was a function of N only, over the entire range of N. We concluded from

this that the oscillations were not an important factor in determining the steady drag. The converse is not necessarily true and more quantitative wake measurements appear to be required if one is to more fully understand this interesting observation.

We suggest a steady model, but realize that our support is based on incomplete evidence. Complete justification of the use of this model could follow only from further measurements of wake structure or a self-consistent analytic solution based on the model. We can not present either here, but suggest the former as being the most likely of success. We will, nevertheless, propose a steady model which we hope would contain the dominant features of the flow. The experiment suggests at least one range of parameters where such a model might be simple. This range was discussed in the introduction as being one that has not been emphasized in the literature:

$$Re \gg 1 , \quad N/Re \ll 1 , \quad Prm \ll 1 , \quad Rm \ll 1 , \quad N \gg 1 \tag{11}$$

With the additional information derived from this experiment, it is hoped that further theoretical progress can be made for this case. The key results which would have to be an integral part of such a theory would be:

$$a_1) \quad C_D \backsim \sqrt{N} \ . \tag{12}$$

b) C_D is insensitive to shape of the body.

CHAPTER VI

Theoretical Discussion

Our objective is to provide a theoretical model which will include the results (12) under the conditions (11). Unfortunately, we have not succeeded in this although certain general concepts can be exposed. Our purpose then is to present a picture of the relevant problem and a possible physical model.

We suggest that for high N, finite disturbances in the velocity can propagate along the magnetic field to large distances by means of weakly damped Alfvén waves. Stewartson (7), (14) proposes that for $\alpha^2 >> 1$, $N \to \infty$, such waves can bring the flow to rest within the area projected by the body in the direction of the applied magnetic field. Consequently, the final steady flow is characterized by stagnant regions extending to infinity upstream and downstream of the body. We consider a flow configuration for finite but large N which involves stagnant regions of finite length and ask: How long will such regions be, and what will the pressures be in them?

Let us first consider the question of Alfvén wave propagation for finite N. In low N experiments such as that of Ahlstrom (22) or Motz (23), propagation of Alfvén waves can play no role. Motz has shown that one can safely use the local potential flow field in calculating currents and body forces. On the other hand, if $N >> 1$, Alfvén wave propagation is almost ideal in an unbounded fluid and must be important in setting up any final steady state from a fluid initially at rest. Lundquist (38) points out that the necessary condition for the existence

of undamped Alfvén waves in a medium of infinite extent is

$$\omega << \frac{B_o^2 \sigma}{\rho} \tag{13}$$

If we substitute $\omega = V_o/d$ as an effective frequency for the initial motion of a body, this condition becomes

$$N >> 1 \tag{14}$$

Lundquist and Lehnert (39) consider the problem of torsional waves set up in a tank by a rotating plate for both mercury and sodium. In their problem the currents flow radially and the condition $J = 0$ at insulating walls results in an additional mechanism for dispersion. Lundquist shows that low frequencies are strongly damped since the corresponding wave lengths normal to the applied field are larger than the dimension of the apparatus and gives the additional condition:

$$\frac{1}{D^2 \sigma \mu \omega} << 1 \tag{15}$$

where D is a length on the order of the dimension of the apparatus normal to the applied field. He combines conditions (12) and (14) to give the requirement:

$$L^2 = \frac{B_o^2 \sigma^2 D^2 \mu}{\rho} >> 1 \tag{16}$$

The number $L = \frac{B_0 \sigma D \sqrt{\mu}}{\sqrt{\rho}}$ can be interpreted as a magnetic Reynolds number based on the Alfvén speed rather than the fluid free stream speed, and has been called the Lundquist number (40).

It is not clear to this author that the Lundquist number is an important parameter in high N flows over bodies. This thought is based on the above model that involves disturbances strongly constrained to the projected area of the body, in the direction of the field. If such a model is correct, the only important boundary condition is fluid dynamic, no flow normal to the walls. In such a case condition, (14) rather than (16) is appropriate. The experiment confirms this since N alone appears to be the important parameter and a simple blockage correction is adequate for $N > 10$. We must emphasize though that for our experiment $L \sim 1$ and one would have to carry out a similar experiment for $L << 1$, $N >> 1$ to show that L does not enter. Such an experiment might be carried out in mercury since, for the same field strength and length scale, $L_{sodium} \lesssim 35\, L_{mercury}$. Since the fluid velocity does not enter into L, the same value of N could be obtained but at a lower value of L.

If we allow that slightly diffused Alfvén waves can exist, what support is there for a description of the flow field which involves such large stagnant regions? First, such a model would explain the experimental result that C_D is insensitive to the shape of the body for large N. Second, we think that work in rotating flows lends support to such an idea. Many authors have suggested that certain analogies can exist between the two problems. One case in particular is quite similar,

that being for strong rotation, slow flow, so that:

$$(\text{Ekman number})^{-1} = \text{coriolis force/viscous force} = \frac{2\Omega d^2}{\nu} >> 1$$

$$(\text{Rossby number})^{-1} = \text{coriolis force/inertial force} = \frac{\Omega d}{V_o} >> 1$$

In that case the results for flow about a body are summarized in the Taylor-Proudman theorem (41): "All slow steady motions in a rotating fluid are two-dimensional." Hide and Roberts (42) state that the analogy is not complete, but this seems to be a result of the order of which they take the strong field, inviscid limits in the MFD case. Gourdine (8), on the other hand, utilizes field splitting prior to taking this limit and avoids the ambiguity of taking limits in one equation which involves two dissipation mechanisms. The result is given in equations (3)-(5) and for $N \longrightarrow \infty$, $Re \longrightarrow \infty$ is:

$$\frac{\partial u_{1,2}}{\partial x} = 0$$

which is identical to the conclusion in the rotating case. Recent experimental evidence due to T. Maxworthy (private communication) lends additional support to this model for rotating flows. He has found that spheres moving through strongly rotating flows do show such stagnant regions. It is hoped that detailed measurements of the flow field as well as the drag in that case will assist in our understanding of the MFD problem.

Let us consider the two-dimensional problem of steady flow over a finite conductivity body which contains no sources or sinks of magnetic field. Since the problem is steady, $\nabla \times E = 0$, and it follows from conditions at infinity that E is a constant equal to zero throughout the flow field. The tangential electrical field is continuous at the surface of the body, so it must be zero inside. Hence,no current flows inside the body and the Lorentz force does not contribute directly to the force on the body. The body force does affect the pressure distribution though, and thusly the drag of the body.

We begin with the inviscid problem for N large, but finite, and will show that in order to have a consistent picture including arbitrarily large drag, non-zero viscosity will again be required. In the limit

$$Rm \to 0 \ , \quad N \to \infty \ , \quad Re \to \infty$$

we consider the thin dissipation layers which separate the stagnant regions from the undisturbed outer flow. We write the variables

$$x = \tilde{x} = O(1) \ ; \quad (y-1) = \tilde{y}/f(N) = O\ (1/f(N))$$

$$V_x = \tilde{V}_x = O(1) \ ; \quad V_y = \tilde{V}_y/f(N) = O\ (1/f(N))$$

$$B_x = \tilde{B}_x = O\ (1) \ ; \quad B_y = \tilde{B}_y/f(N) = O\ (1/f(N))$$

$$P = g(N)\ \tilde{P} = O\ (g(N))$$

where all tilde quantities are $O(1)$, and $f^{-1}(N)$ and $g(N)$ give the order of the layer thickness and pressure. We assume that $f(N) \to \infty$ as $N \to \infty$, and since $Rm \to 0$, that the magnetic field is only slightly disturbed. We take a linear approximation for the magnetic field:

$$\begin{aligned} \tilde{B}_x &= 1 + \gamma\, b_x \\ \tilde{B}_y &= \gamma\, b_y \\ \gamma &\ll 1 \end{aligned} \tag{17}$$

The induction equation (1b) yields

$$\begin{aligned} \frac{\partial b_x}{\partial \tilde{y}} &= \tilde{V}_y \\ \gamma &= Rm/f(N)^2 \end{aligned} \tag{18}$$

The momentum equation becomes:

$$\left(\tilde{V}_x \frac{\partial}{\partial \tilde{x}} + \tilde{V}_y \frac{\partial}{\partial \tilde{y}}\right) \tilde{V}_x + g(N) \frac{\partial \tilde{p}}{\partial \tilde{x}} = -N \frac{Rm}{f(N)^4} b_y \tilde{V}_y \tag{19}$$

and

$$\left(\tilde{V}_x \frac{\partial}{\partial \tilde{x}} + \tilde{V}_y \frac{\partial}{\partial \tilde{y}}\right) \frac{\tilde{V}_y}{f(N)} + f(N)\, g(N) \frac{\partial \tilde{p}}{\partial \tilde{y}} = \frac{-N}{f(N)} \tilde{V}_y \tag{20}$$

The inertial term in (20) can be neglected for a thin layer and the pressure gradient across the layer is balanced by the body force; as $N \to \infty$:

$$\frac{\partial \tilde{P}}{\partial \tilde{y}} = -\tilde{V}_y$$
$$g(N) = N/f(N)^2 \qquad (21)$$

By combining with (18), we get

$$\frac{\partial}{\partial \tilde{y}} (\tilde{P} + b_x) = 0 \qquad (22)$$

which is analogous to the condition of constant pressure across an ordinary viscous boundary layer. Since $Rm \to 0$, (19) becomes

$$(\tilde{V}_x \frac{\partial}{\partial \tilde{x}} + \tilde{V}_y \frac{\partial}{\partial \tilde{y}}) \tilde{V}_x + g(N) \frac{\partial \tilde{P}}{\partial \tilde{x}} = 0 \qquad (23)$$

In order to choose $g(N)$, we must consider the consequences of the non-linear equation for the Bernoulli function (9).

$$\bar{V} \cdot \nabla H = -(\alpha^2/Rm) J^2$$

We see that the Bernoulli function H is strictly decreasing along streamlines that pass through any regions of current. Along the center streamline $J = 0$, from symmetry, and the Bernoulli function is constant up to the face of the body. Consequently, the maximum pressure on the front of the body is stagnation pressure and within the stagnant region $\nabla P = 0$.

For $\alpha^2 \gg 1$ and any N, Joule losses provide a dissipation mechanism within the forward wake and undisturbed conditions exist at infinity upstream. The non-linear dissipation mechanism which results in a change in the Bernoulli function can exist within the thin layers described. Any streamline that passes through such a layer will reach downstream infinity, resulting in a distribution of Bernoulli function there. The linearized equations apply far downstream but allow for only exponentially small currents outside of the parabolic wake which lies upstream for $\alpha^2 > 1$. Parallel flow is reached if we go far enough downstream for any finite N. If we require uniform pressure at infinity, a non-zero $\frac{\partial V_{II}}{\partial \tilde{x}}$ exists there, and this is termed a "non-diffusive vortex trail" by Tamada.

Let us consider a model consistent with these requirements. We choose

$$\begin{aligned} f(N) &= \sqrt{N} \\ g(N) &= 1 \end{aligned} \tag{24}$$

giving

$$\left(\tilde{V}_x \frac{\partial}{\partial \tilde{x}} + \tilde{V}_y \frac{\partial}{\partial \tilde{y}}\right) \tilde{V}_x + \frac{\partial \tilde{P}}{\partial \tilde{x}} = 0 \tag{25}$$

and

$$\frac{\partial \tilde{P}}{\partial \tilde{y}} = -\tilde{V}_y = -\frac{\partial b_x}{\partial \tilde{y}} \tag{26}$$

Such layers are suggested by Childress (12) for $N/Re << 1$ but never used in his later work. Let us consider the maximum drag which such a model would provide. As upstream, the Bernoulli function is conserved along the center streamline downstream. If we require uniform pressure at infinity, the Bernoulli function can never be negative, and the base pressure is constant equal to zero (relative to P_o) within a stagnant region.

Dissipation layers spreading like $1/\sqrt{N}$ extend only upstream, and the mathematical description of the flow field would have to be completed by describing the matching of such layers to the upstream wake which also spreads like $1/\sqrt{N}$. Since the pressure is everywhere uniform downstream, no current flows and the linear approximation is valid everywhere except possibly at the edges of the body. The magnetic field is uniform downstream and equal to its undisturbed value. We can integrate (22) and determine the constant at $\tilde{y} \to \infty$. We then have the field distribution in the layer from the solution for the pressure. The determination of the magnetic field is completed by matching the layer solution to a potential distribution in the stagnant region and body.

The consequence of this model is that the maximum drag coefficient equals one. Childress (43) utilizes a successive approximation technique and only considers terms of the first order in solving equations (25)-(26). He finds C_D (first approximation) = .721 . It seems clear that for finite N , inviscid, steady flow, we can not account for the large drag measured. The model we have described for the flow upstream seems to be on firm ground, but we need to propose another model for the

downstream flow.

In order to have drag which increases with $\sqrt{N}$, we must allow $g(N) = \sqrt{N}$ on the body. Since the maximum pressure on the front face is stagnation pressure, we must have an increasingly large suction on the back as N increases. Making this assumption, we get

$$\begin{aligned} g(N) &= \sqrt{N} \\ f(N) &= N^{\frac{1}{4}} \end{aligned} \tag{27}$$

and the equations

$$\frac{\partial \tilde{P}}{\partial \tilde{x}} = 0 \tag{28}$$

and

$$\frac{\partial \tilde{P}}{\partial \tilde{y}} = -\tilde{V}_y = -\frac{\partial b_x}{\partial \tilde{y}} \tag{29}$$

We note that the only difference between the equations valid for layers of thickness $1/\sqrt{N}$ and the equations valid for layers $1/N^{\frac{1}{4}}$ is the existence of the inertial term in equation (25). The solution to equations (28), (29), along with the continuity equation, includes two undetermined functions $\tilde{P}(\tilde{y})$ and $\tilde{P}_1(\tilde{y})$:

$$\begin{aligned} \tilde{V}_y &= -\frac{d\tilde{P}}{d\tilde{y}} \\ \tilde{V}_x &= \tilde{x}\,\frac{d^2\tilde{P}}{d\tilde{y}^2} + \tilde{P}_1 \end{aligned}$$

whereas equations (25) and (26) can in principle provide complete solutions. This difficulty might be resolved by substituting a full expansion for the tilde variables in terms of a small parameter such as $1/\sqrt{N}$, each higher order providing sufficient information to determine the next lower order.

The model we propose is identical on the upstream side to that described by equations (24) - (26) , but differs downstream due to the large but negative pressure inside the stagnant region. For N large but finite, the layers spread and merge at a distance $x = O(\sqrt{N})$ downstream and $x = O(N)$ upstream. The behavior of the far field for N large but finite is describable by the solutions of Gourdine (8). Upstream a wake spreading parabolically like $1/\sqrt{N}$ can be matched to the layer solution, but no diffusion mechanism exists downstream. Since the Bernoulli function is conserved along the center streamline, it must be large and negative at downstream infinity. This is inconsistent with the required far wake behavior.

Such a near field can exist, though, if we relax the condition on Re and only require that Re be large but finite:

$$\mathrm{Re} \gg 1 \quad ; \qquad N/\mathrm{Re} \ll 1$$

We then have a mechanism to permit the pressure to return to P_o and the drag to be distributed as momentum defect in the viscous wake. For N finite we are still faced with the difficult problem of matching the layer solution with the viscous wake. However, a rather simple flow results for $N \to \infty$ while still maintaining the condition $N/\mathrm{Re} \ll 1$.

The layers become infinitesimally thin sheets extending to infinity, and the flow is superficially similar to the infinite conductivity, zero viscosity model proposed by Stewartson (13). In that case infinitely long slugs are formed, both sides of the body contribute equally to the drag, and the drag coefficient is proportional to the Alfvén number. Here we find that for:

$$N \to \infty$$

$$Re \to \infty$$

$$N/Re \to 0$$

that

$$C_D \sim \sqrt{N}$$

and the large drag is due to suction on the base. The pressure jump across the layer tends to infinity with $\sqrt{N}$, and is balanced by current flowing in the thin layer which interacts with the applied field. The current is estimated for finite N to be:

$$J \sim \frac{\Delta B_x}{\Delta y} \sim 0\,(Rm/N^{\frac{1}{4}})$$

and for $Rm \to 0$, $N \to \infty$:

$$J \to 0$$

The ultimate flow for $N \to \infty$ is shown in figure 22.

Initial measurements, carried out by T. Maxworthy (private communication), of the pressure distribution on a sphere for high N show excellent agreement with the drag measurement. They show that the drag is in fact due to low base pressures, but do not in themselves confirm or deny the model proposed here.

The question of how viscosity enters for large but finite N seems to have features in common with the ordinary high Re problem of separated steady flow, which is itself unresolved (44). The problem here is different in that the separation and the base pressure are governed by another body force. In both cases we must connect a boundary layer solution with the viscous wake through a rather poorly understood intermediate region. We expect that progress in either problem would be beneficial to the other, but are unable to make that contribution here.

CHAPTER VII

Conclusion

In our survey of the literature of this field, we noted that many authors have chosen to emphasize what are clearly non-physical problems. There seemed to be a tendency to treat MFD problems as of an exceptional nature and to divorce ones thinking not only from physical MFD flows, but from other problems in fluid mechanics as well. On the other hand, consideration of the physically realizable cases led to a definitive set of conditions and to similarities with two other areas of fluid mechanics currently under investigation. These were strongly rotating flows and steady high Re flows. One must be careful in carrying over exact results from one problem to another, but a successful approach in one might prove to be fruitful in the others.

A measurement of the drag coefficient of spheres and disks was carried out over a fairly wide range of N. We found that the sphere C_D was not a function of N for $N \lesssim .3$, began to increase appreciably for $N \sim 1$, and reached an asymptotic dependence proportional to $\sqrt{N}$ for $N \sim 10$. The disk C_D was relatively unchanged for $N < 10$, began to increase for $N \sim 10$, and for $N > 20$ the drag for spheres and disks was approximately the same. We concluded that the high N range was characterized by C_D insensitive to body shape. The intermediate range $(1 \leq N \leq 10)$ did not give any simple dependence on N, and we expect that the physical situation involves a complex combination of both viscous and Lorentz forces. We chose to emphasize the high N behavior because of its simplicity.

We noted the analogy between the Taylor-Proudman theorem for strong rotation and similar results for high N flows. This suggested a physical model involving large stagnant regions both upstream and downstream of the body. Equations were presented to describe thin dissipation layers separating the inner stagnant region from the uniform outer flow. The similarity between these Joule dissipation layers for high N and viscous dissipation layers for ordinary high Re flows became apparent. Finally, the importance of matching the near field to a viscous wake downstream appeared, and we pointed out that this unanswered question was crucial to both steady high Re flows and high N flows. We expect that such a physical model should be amenable to a theoretical analysis. We suggested a singular perturbation technique similar to that used by others, but were unable to provide a solution here. We feel that work should continue both on this theoretical approach and on further measurements. Detailed flow and field measurements in the vicinity of the body would be particularly useful and we intend to pursue such an experimental program.

This experiment is to our knowledge the first successful measurement of a gross physical quantity for MFD flows with strong interaction. In itself, it has solved few, if any, of the many unanswered questions which have appeared. Its principal value is to lend direction to the research which must continue if one is to understand these phenomena. By demonstrating a physical set of conditions and a consequence of them, we have gained an orientation in our view to this problem. It is hoped that because of this, further advance can be made.

References

1. Sears, W. R. and Resler, E. L., "Magneto-Aerodynamic Flow Past Bodies," Advances in Applied Mech., Vol. 8, 1-68, 1964.
2. Liepmann, H. W., Hoult, D. P., and Ahlstrom, H. G., "Concept, Construction, and Preliminary Use of a Facility for Experimental Studies in Magneto-Fluid Dynamics," Miszellaneen Angewandten Mechanick, 175-189, 1960, Acad. Verlag, Berlin.
3. Childress, S., "On the Flow of a Conducting Fluid of Small Viscosity," Proc. of a Symposium on Fundamental Topics in Relativistic Fluid Mechanics and Magnetohydrodynamics, Academic Press, 1963.
4. Resler, E. L. and McCune, J. E., "Some Exact Solutions in Linearized Magnetoaerodynamics for Arbitrary Magnetic Reynolds Numbers," Rev. Mod. Phys. 32 (848-854) 1960.
5. Stewartson, K., "Magneto-Fluid Dynamics of Thin Bodies in Oblique Fields - I," Zeits. f. angew. Math. und Phys. 12, 261-271 (1961).
6. Ludford, G. S. S., "The Effect of a Very Strong Magnetic Cross-Field on Steady Motion through a Slightly Conducting Fluid," J. Fluid Mech. 10, 141-155 (1961).
7. Stewartson, K., "Magneto-Fluid Dynamics of Bodies in Aligned Fields," Proc. Roy. Soc. A 275, 70-86 (1963).
8. Gourdine, M., "Magnetohydrodynamic Flow Constructions with Fundamental Solutions," J. Fluid Mech. 10, 459-465 (1961).
9. Gourdine, M., "On the Role of Viscosity and Conductivity in Magnetohydrodynamics," JPL Tech. Rept. 32-3, 1960.

10. Chester, W., "The Effect of a Magnetic Field on the Flow of a Conducting Fluid Past a Body of Revolution," J. Fluid Mech. 10, 459-465 (1961).

11. Chang, I., "On a Singular Perturbation Problem in Magnetohydrodynamics," Zeits. f. angew. Math. und Phys. 14, 134-147 (1963).

12. Childress, S., "The Effect of a Strong Magnetic Field on Two-Dimensional Flows of a Conducting Fluid," J. Fluid Mech. 15, 429-441 (1963).

13. Stewartson, K., "On the Motion of a Non-Conducting Body through a Perfectly Conducting Fluid," J. Fluid Mech. 8, 82-96 (1960).

14. Stewartson, K., "Motion of Bodies through Conducting Fluids," Rev. of Mod. Phys. 32, 855-859 (1960).

15. Sears, W. R. and Resler, E. L. Jr., "Theory of Thin Airfoils in Fluids of High Electrical Conductivity," J. Fluid Mech. 5, 257-273 (1959).

16. Ludford, G. S. S. and Leibovich, S., "The Transient Hydromagnetic Flow Past an Airfoil for an Aligned Magnetic Field," Journal de Mécanique 4, 21-50 (1965).

17. Stewartson, K., "On Magnetic Boundary Layers," J. Inst. Maths. Applics. 1, 29-41 (1965).

18. Tamada, K., "Flow of a Slightly Conducting Fluid Past a Circular Cylinder with Strong, Aligned Field," Phys. of Fluids 5, 817-823 (1962).

19. Reitz, J. R. and Foldy, L. L., "The Force on a Sphere Moving through a Conducting Fluid in the Presence of a Magnetic Field," J. Fluid Mech. 11, 133-142 (1961).

20. Leonard, B., "Some Aspects of Magnetohydrodynamic Flow about a Blunt Body," AFOSR 2714 (1962).

21. Seebass, R. and Tamada, K., "The Distortion of a Magnetic Field by the Flow of a Conducting Fluid Past a Circular Cylinder," J. Fluid Mech. 22, 561-578 (1965).

22. Ahlstrom, H., "Experiments on the Upstream Wake in Magneto-Fluid Dynamics," J. Fluid Mech. 15, 205-221 (1963).

23. Motz, R. O., "Magnetohydrodynamics of an Oscillating Dielectric Sphere," Plasma Research Laboratory, Columbia University, Report No. 21 (1965).

24. Lary, E. C., "A Theory of Thin Airfoils and Slender Bodies in Fluids of Finite Electrical Conductivity with Aligned Fields," J. Fluid Mech. 12, 209-226 (1962).

25. Suzuki, B., (to be published).

26. Maxworthy, T., "Measurements of Drag and Wake Structure in Magneto-Fluid Dynamic Flow about a Sphere," Heat Transfer and Fluid Mech. Inst., 197-205 (1962).

27. Maxworthy, T., "Liquid Sodium Flow Facility for Magneto-Fluid Dynamic Research," Rev. of Sci. Inst. 32, 1260-1261 (1961).

28. Cowling, T. G., "Magnetohydrodynamics," Interscience (1957).

29. Maxworthy, T., JPL Tech. Rept. (to be published).

30. Shercliff, J. A., "The Theory of Electromagnetic Flow Measurement," Cambridge (1962).

31. Schlichting, H., "Boundary Layer Theory," Fourth Edition, McGraw-Hill (1960).

32. Reshotko, E., "Experimental Study of Stability of Pipe Flow," JPL Progress Report No. 20-364 (1958).

33. Liquid Metals Handbook, Third Edition, Atomic Energy Commission (1955).

34. Maskell, E. C., "A Theory of the Blockage Effects on Bluff Bodies and Stalled Wings in a Closed Wind Tunnel," R.A.E. Report 2685 (1963).

35. Fail, R. A., Lawford, J. A. and Eyre, R. C. W., "Low-Speed Experiments on the Wake Characteristics of Flat Plates Normal to an Air Stream," R. & M. Report 3120 (1959).

36. Goldstein, S., "Modern Developments in Fluid Dynamics," Vol. II, Oxford (1957).

37. Globe, S., "The Effect of a Longitudinal Magnetic Field on Pipe Flow of Mercury," Trans. Amer. Soc. Mech. Eng. 83, Series C, 445-453 (1961).

38. Lundquist, S., "Experimental Investigation of Magneto-Hydrodynamic Waves," Phys. Rev. 76, 1805-1809 (1949).

39. Lehnert, B., "Magneto-Hydrodynamic Waves in Liquid Sodium," Phys. Rev. 94, 815-824 (1954).

40. Cambel, A. B., "Plasma Physics and Magneto-Fluid Mechanics," McGraw-Hill (1963).

41. Squire, H. B., "Rotating Fluids," Surveys in Mechanics, 139-161 (1956).

42. Hide, R. and Roberts, P., "Some Elementary Problems in Magneto-Hydrodynamics," Advances in Applied Mech. 7, 215-316 (1962).

43. Childress, S., "Inviscid Magnetohydrodynamic Flow in the Presence of a Strong Magnetic Field," JPL SPS 37-22, 254-255 (1963).

44. Acrivos, A., Snowden, D. D., Grove, A. S., and Petersen, E. E., "The Steady Separated Flow Past a Circular Cylinder at Large Reynolds Numbers," J. Fluid Mech. 21, 737-760 (1965).

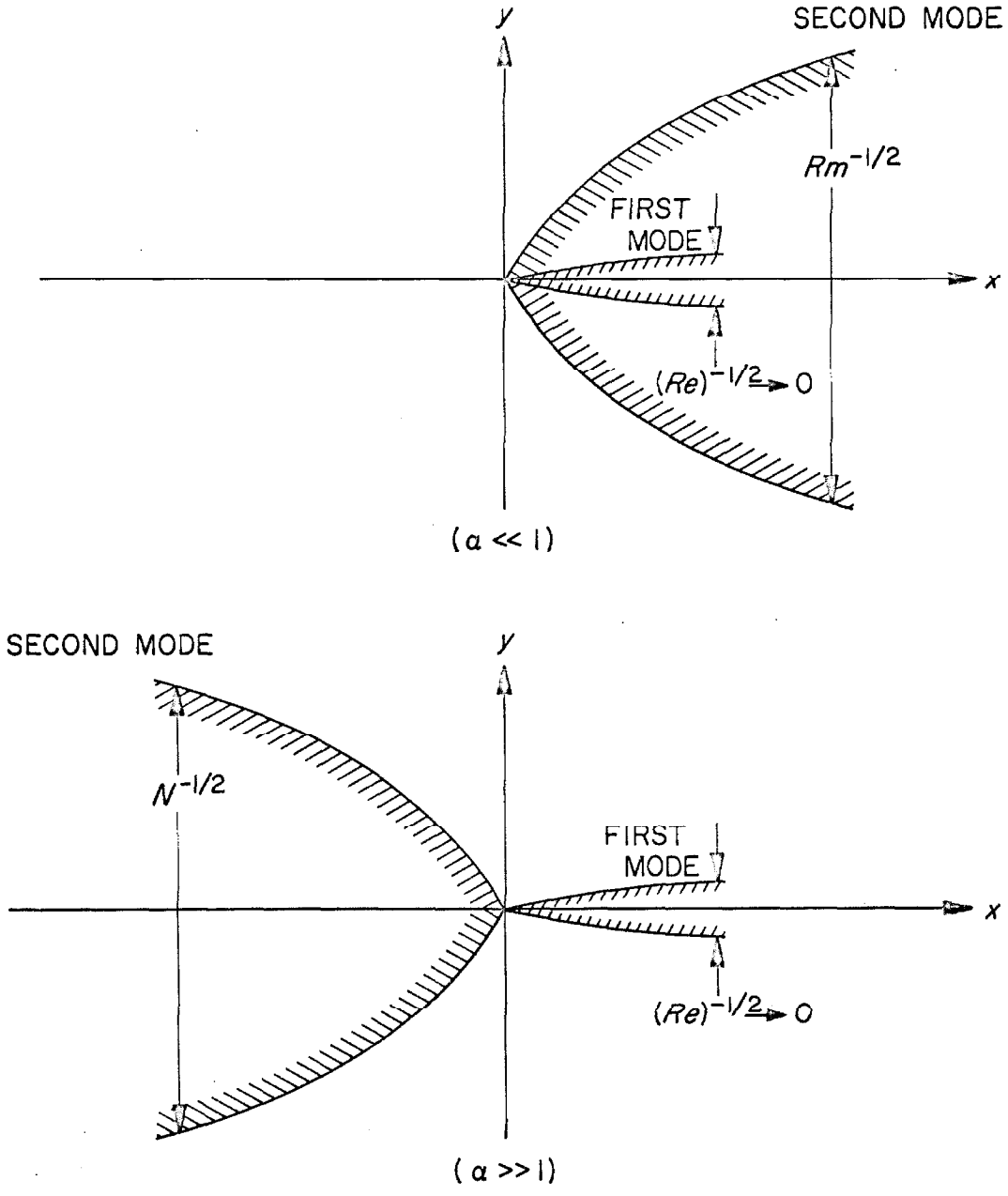

FIG. 1 Wake Behavior for $Pr_m \ll 1$, $N/Re \ll 1$

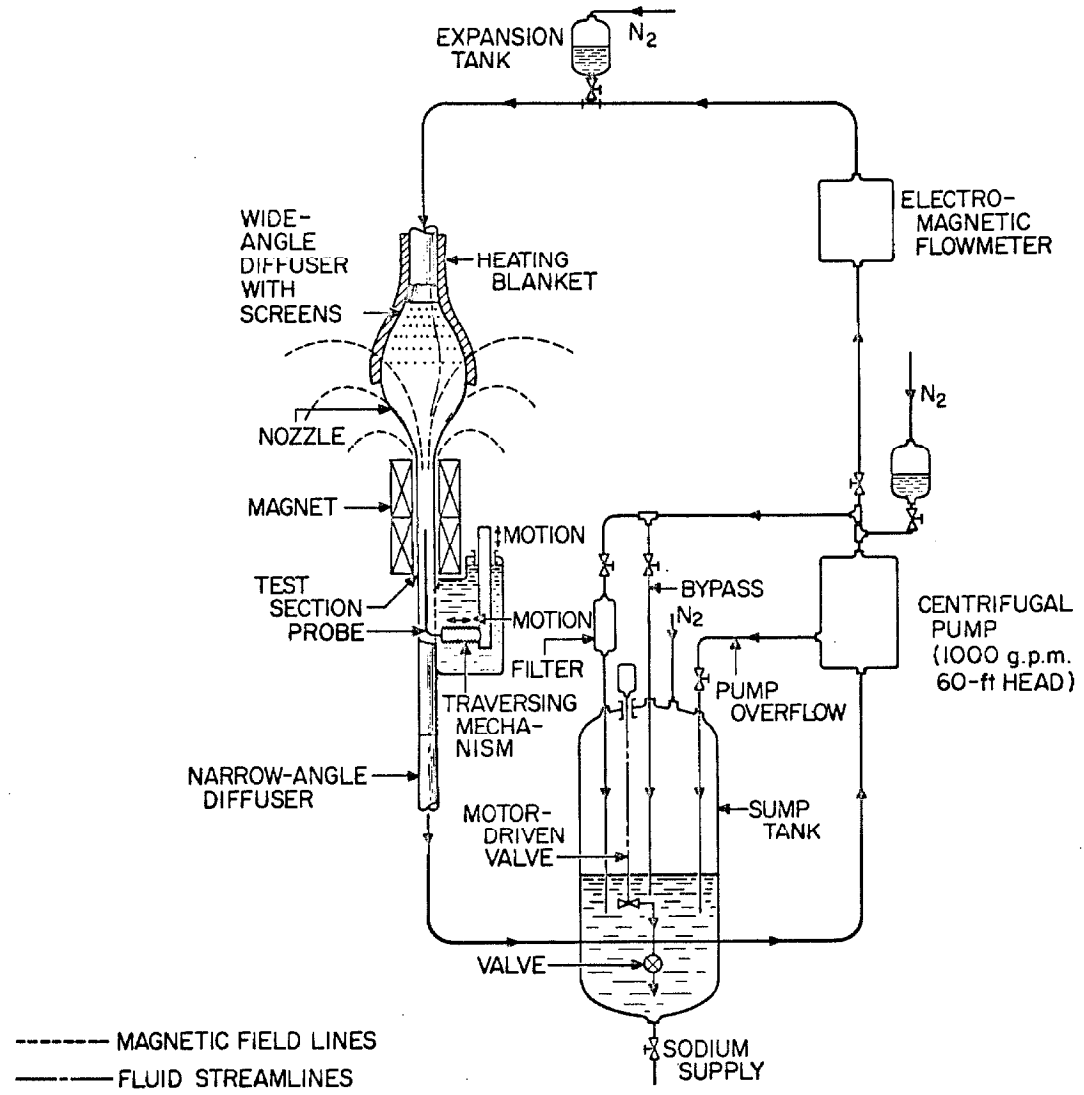

FIG. 2 FLOW DIAGRAM FOR THE J.P.L. LIQUID SODIUM TEST FACILITY

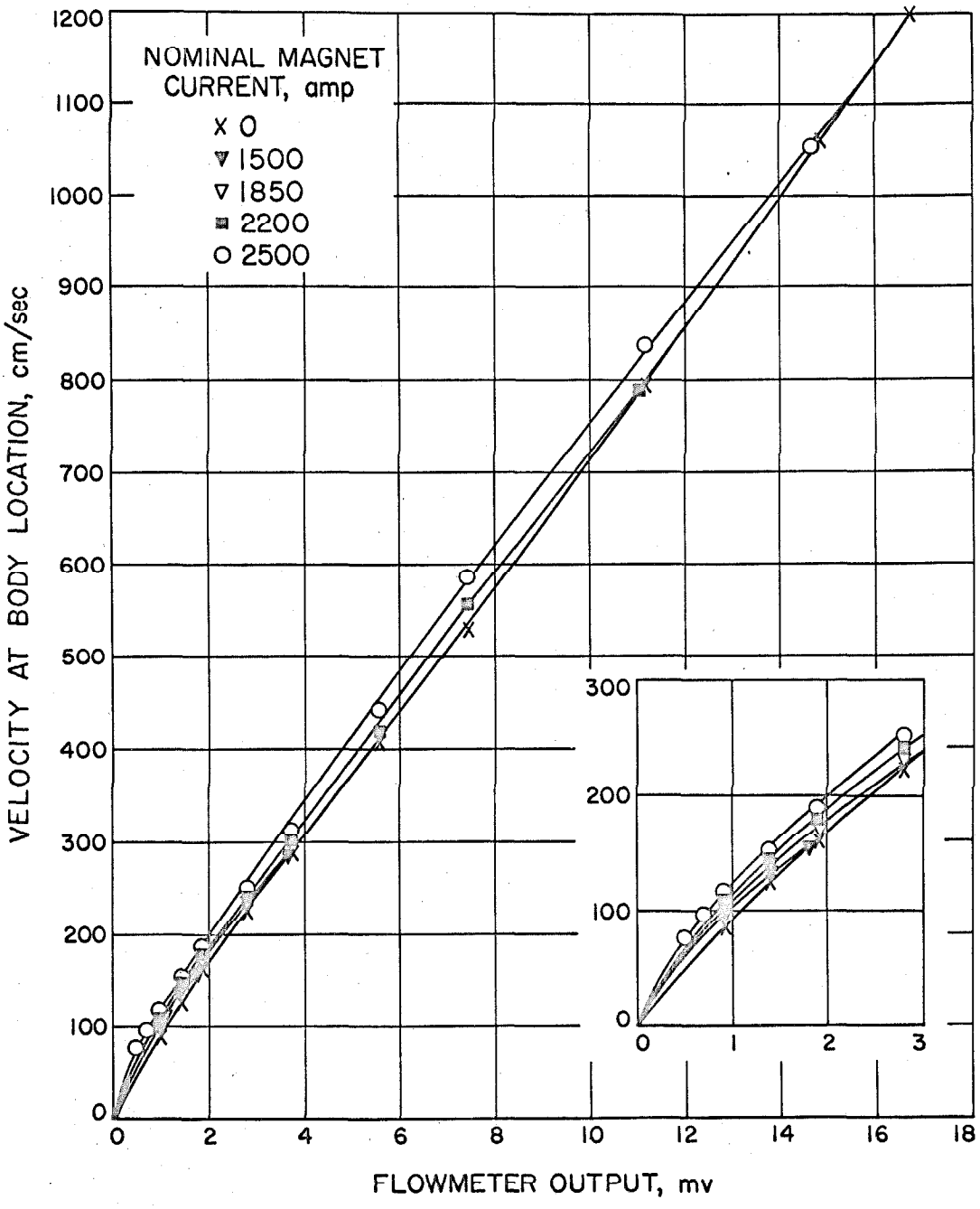

FIG. 3 Flow Meter Calibration

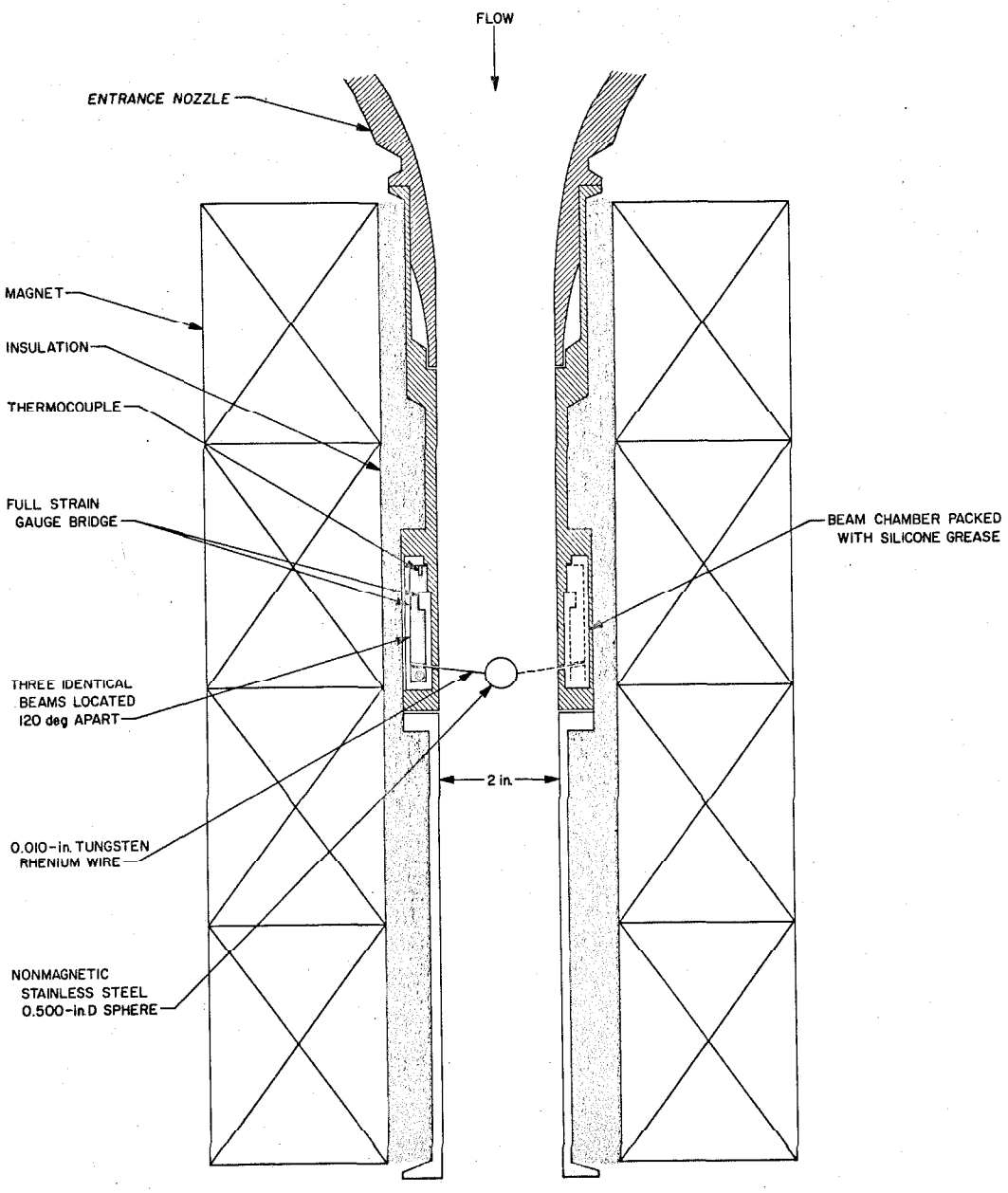

FIG. 4 Drag Balance Test Section

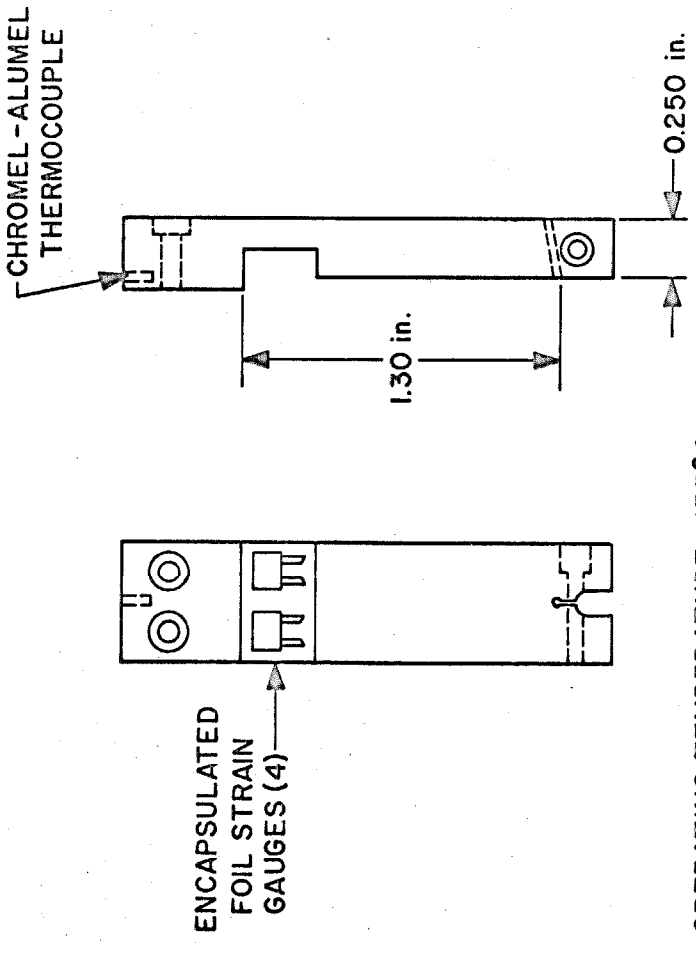

FIG. 5 Strain Gauge Beam

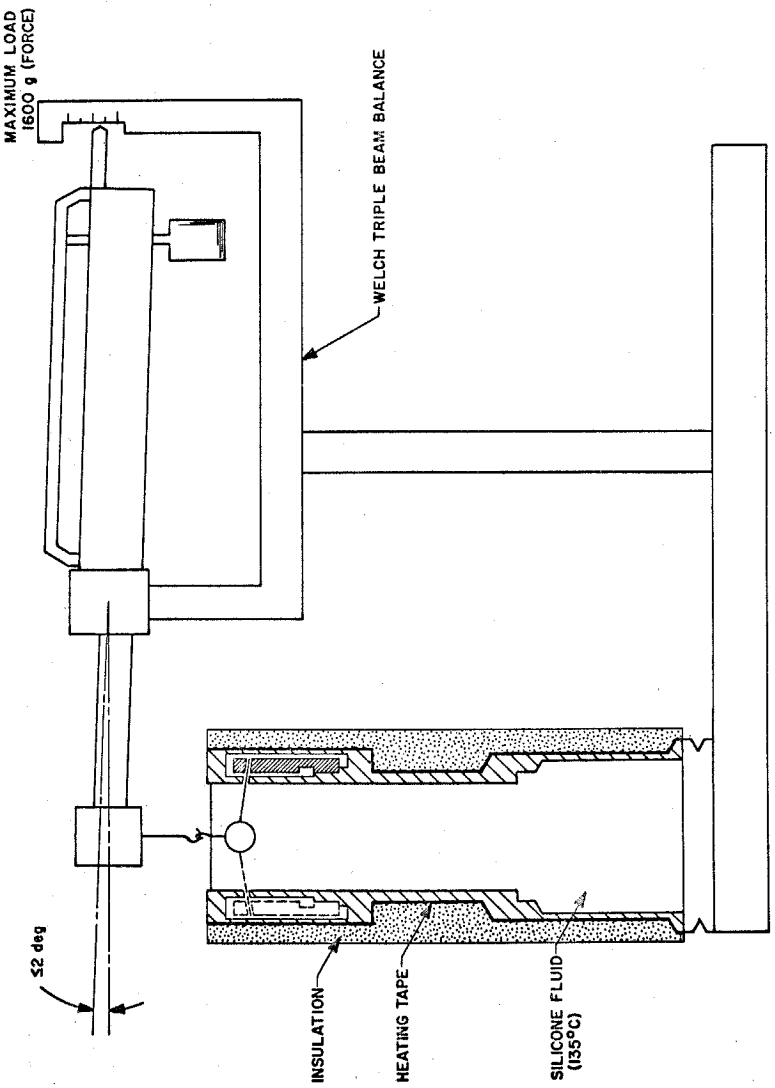

FIG. 6 Calibration Technique

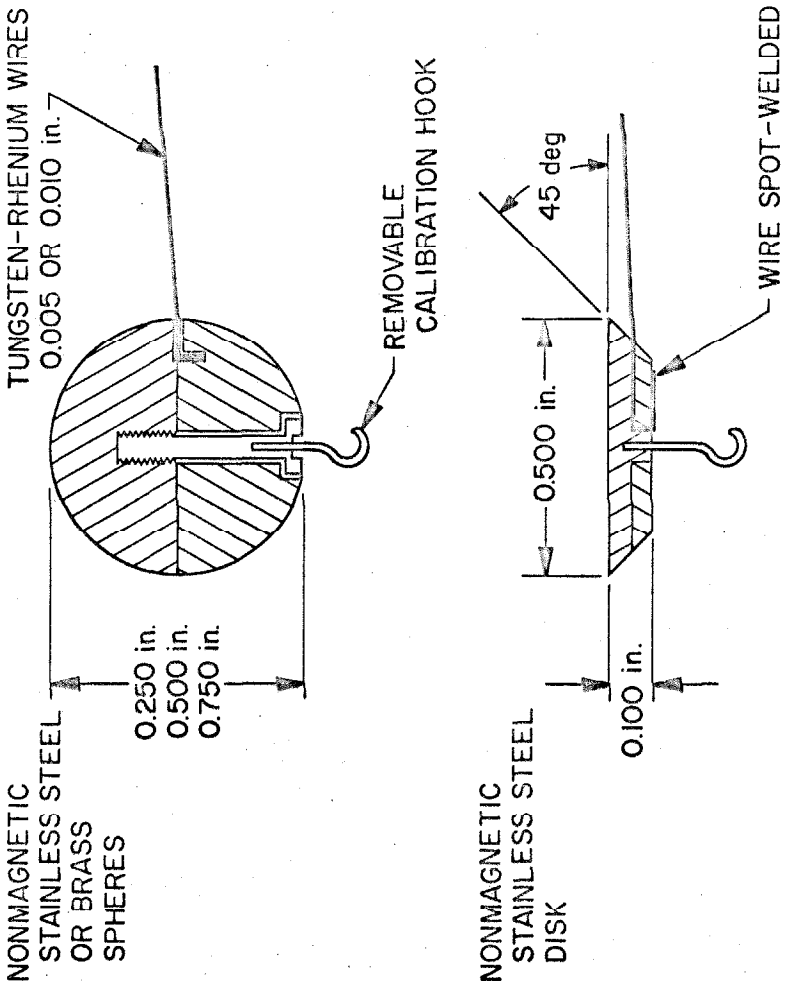

FIG. 7 Model Configuration

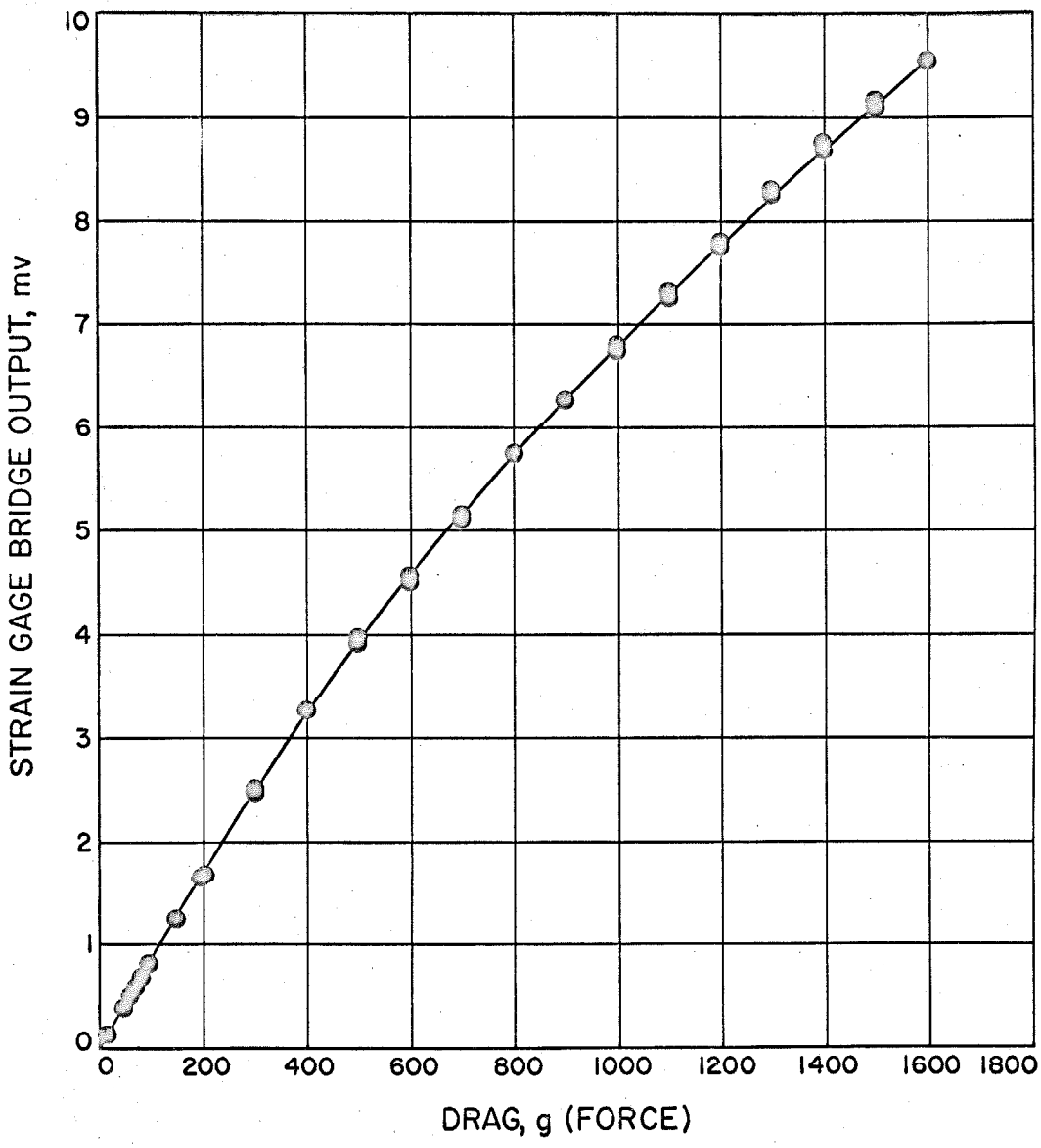

FIG. 8 Drag Balance Calibration; 0.750-In. Sphere

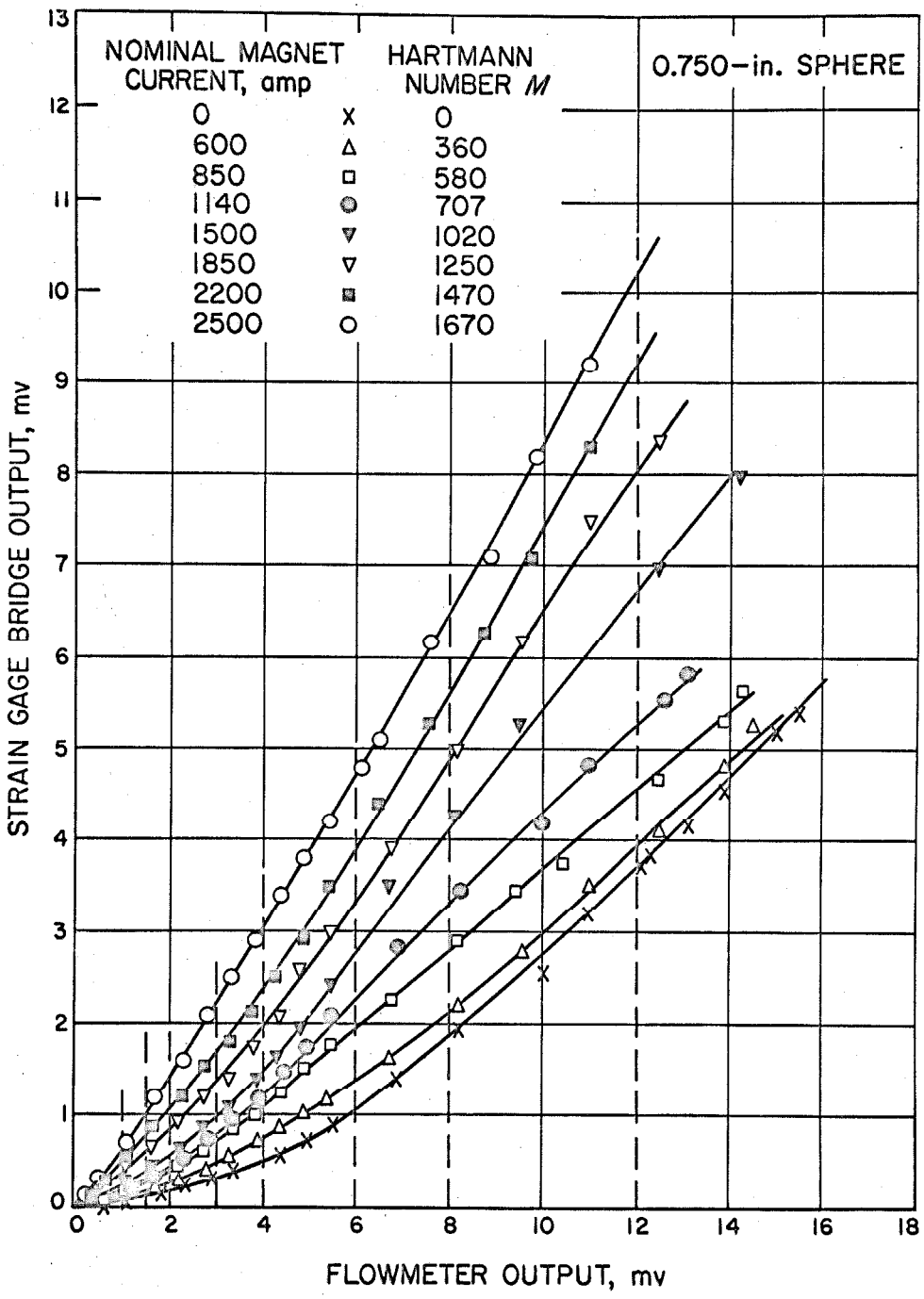

FIG. 9 Raw Data for 0.750-In. Sphere

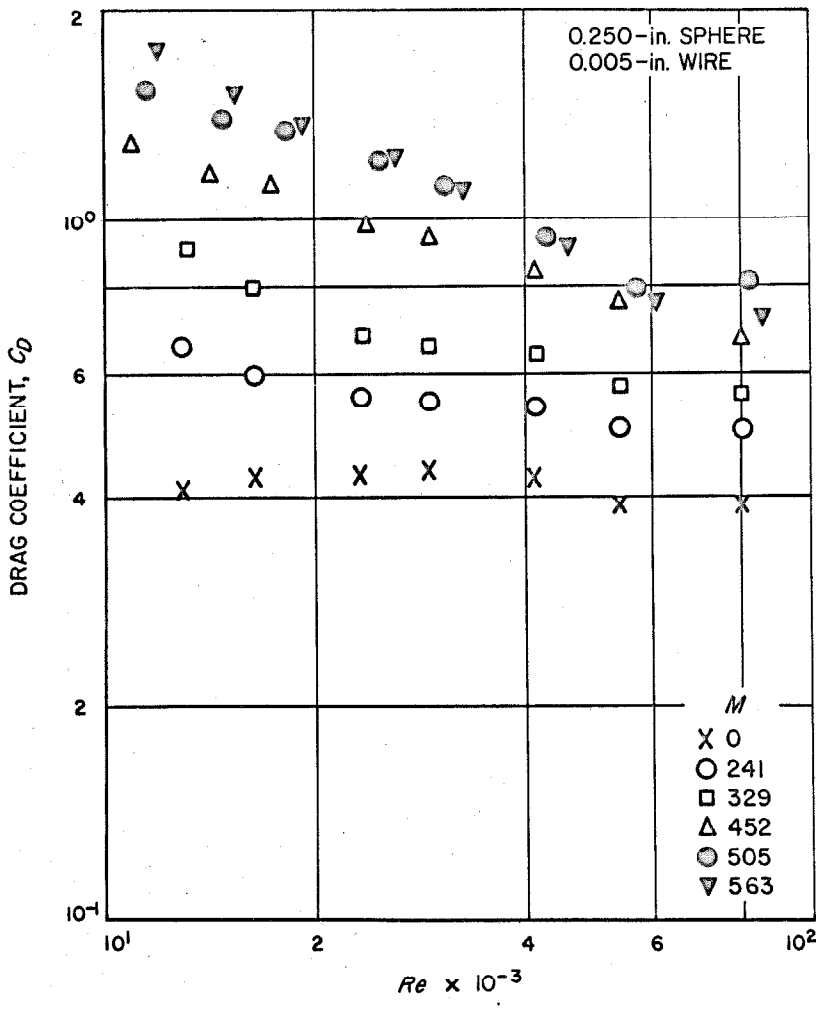

FIG. 10 Drag Coefficient Vs Reynolds Number for 0.250-In. Sphere

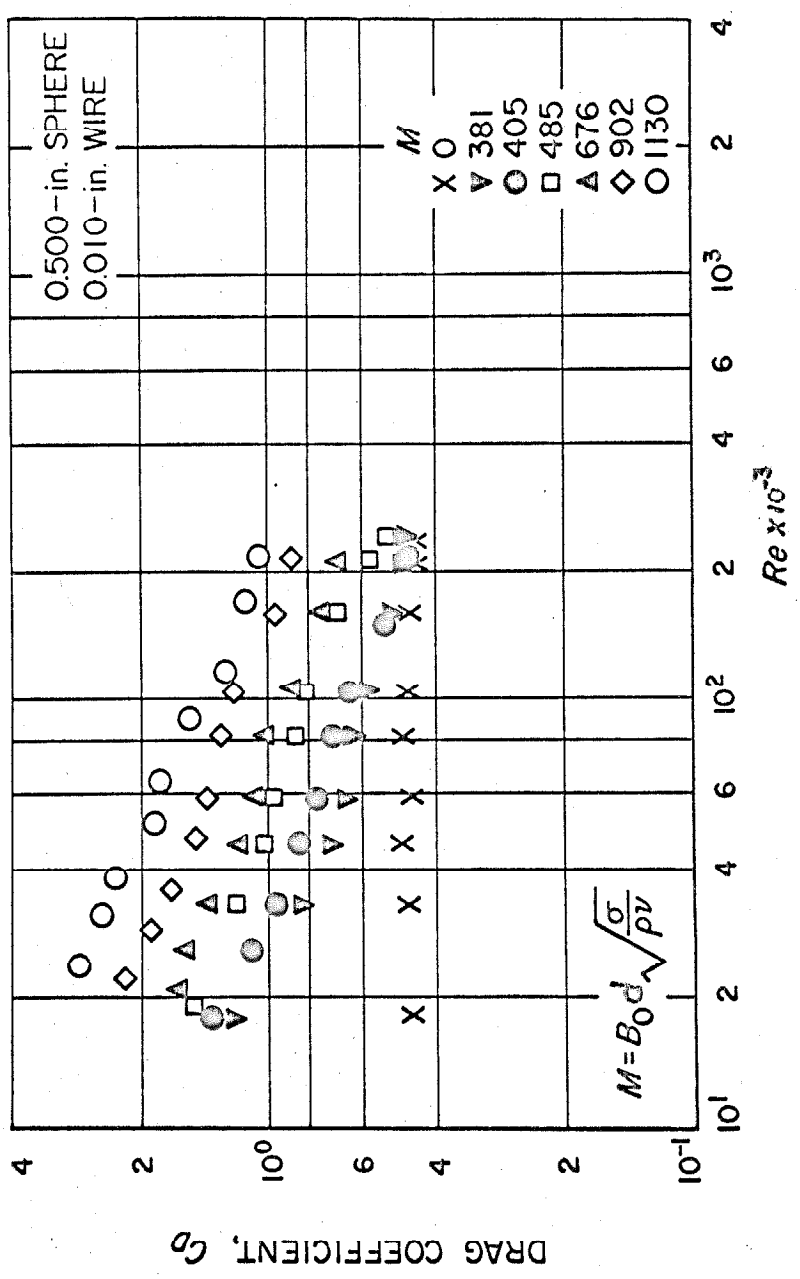

FIG. 11 Drag Coefficient Vs Reynolds Number for 0.500-In. Sphere

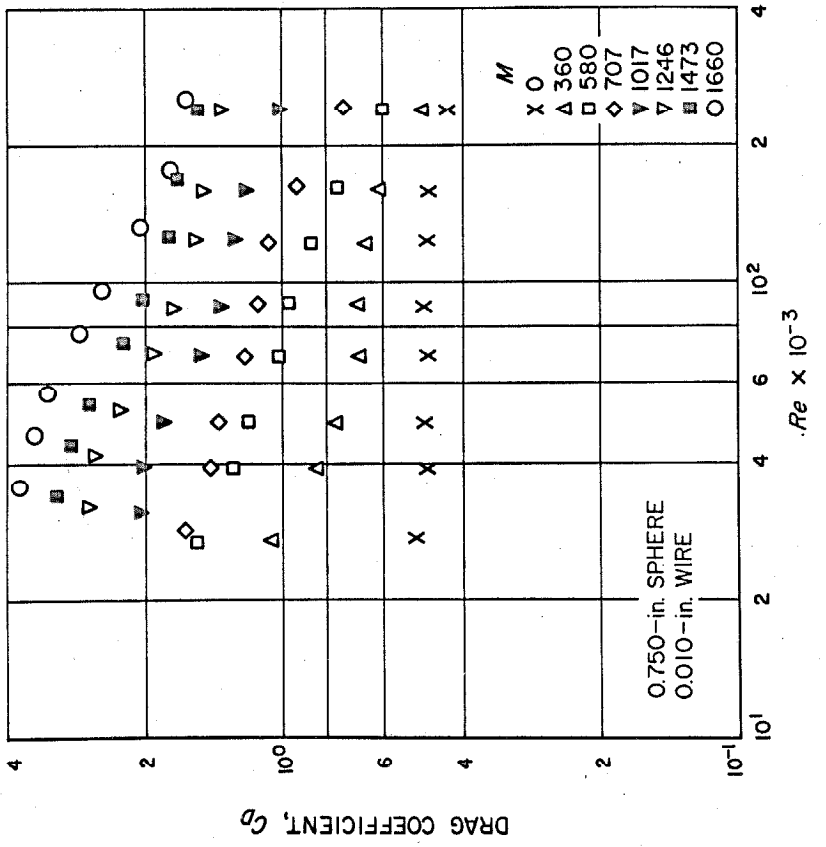

FIG. 12 Drag Coefficient Vs Reynolds Number for 0.750-In. Sphere

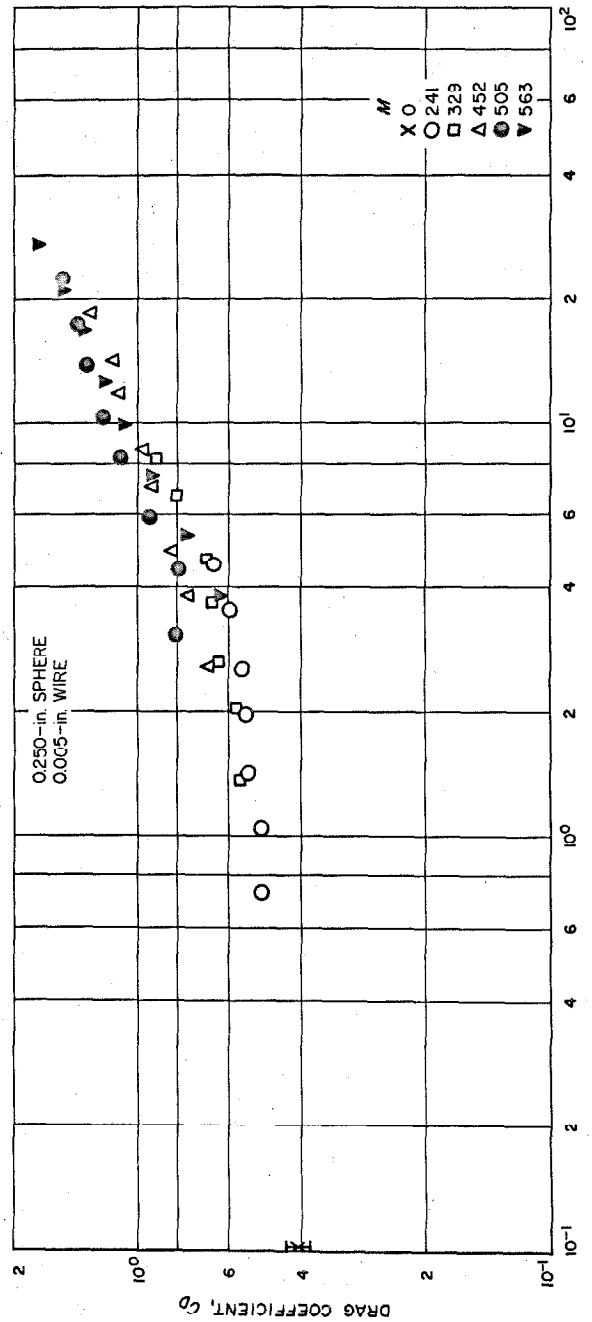

FIG. 13 Drag Coefficient Vs Interaction Parameter for 0.250-In. Sphere

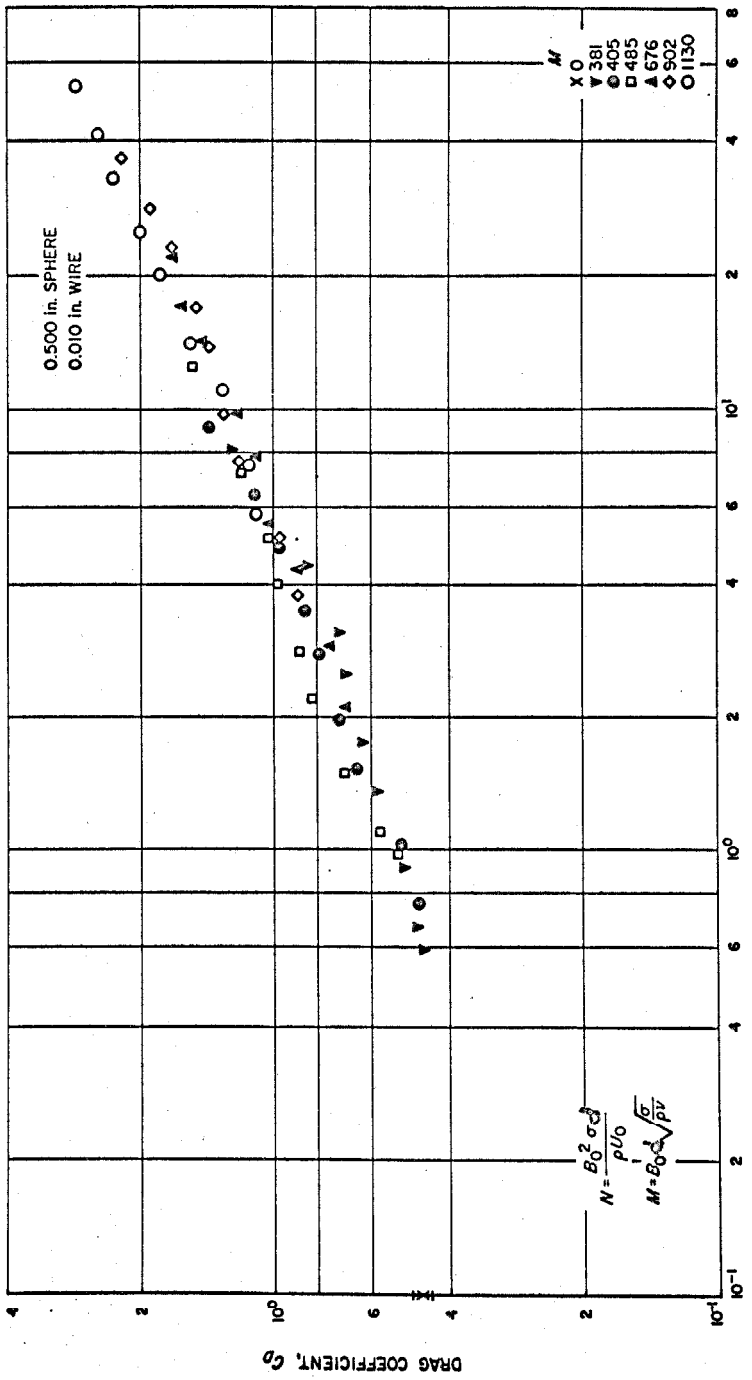

FIG. 14 Drag Coefficient Vs Interaction Parameter for 0.500-In. Sphere

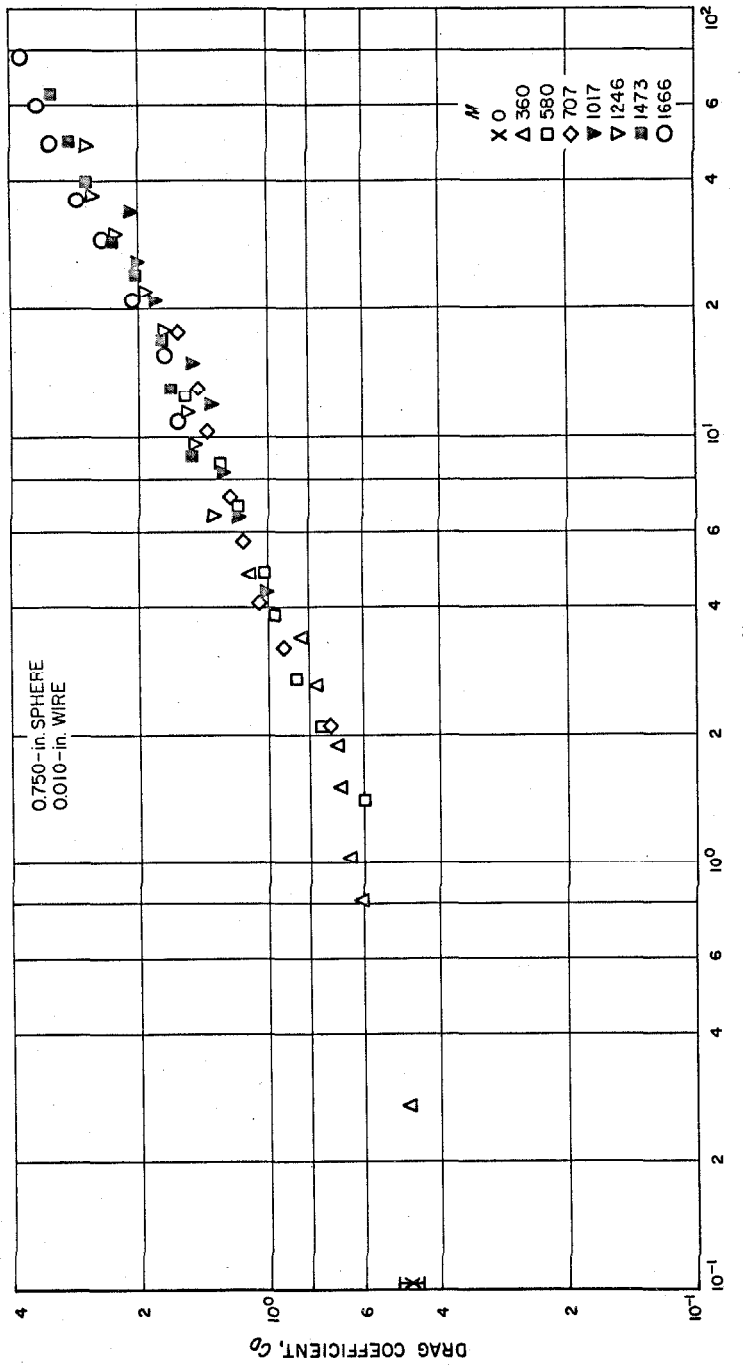

FIG. 15 Drag Coefficient Vs Interaction Parameter for 0.750-In. Sphere

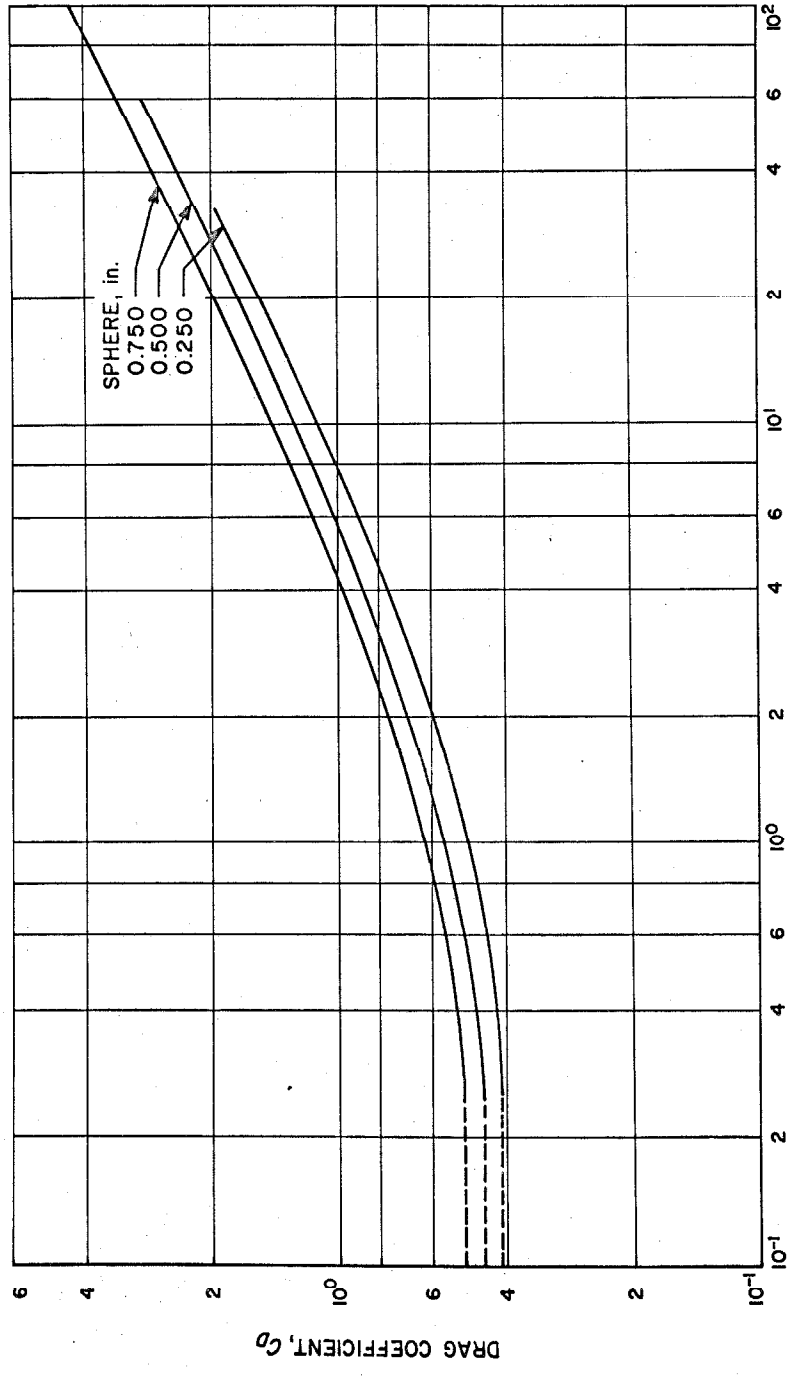

FIG. 16 Drag Coefficient Vs Interaction Parameter for Spheres

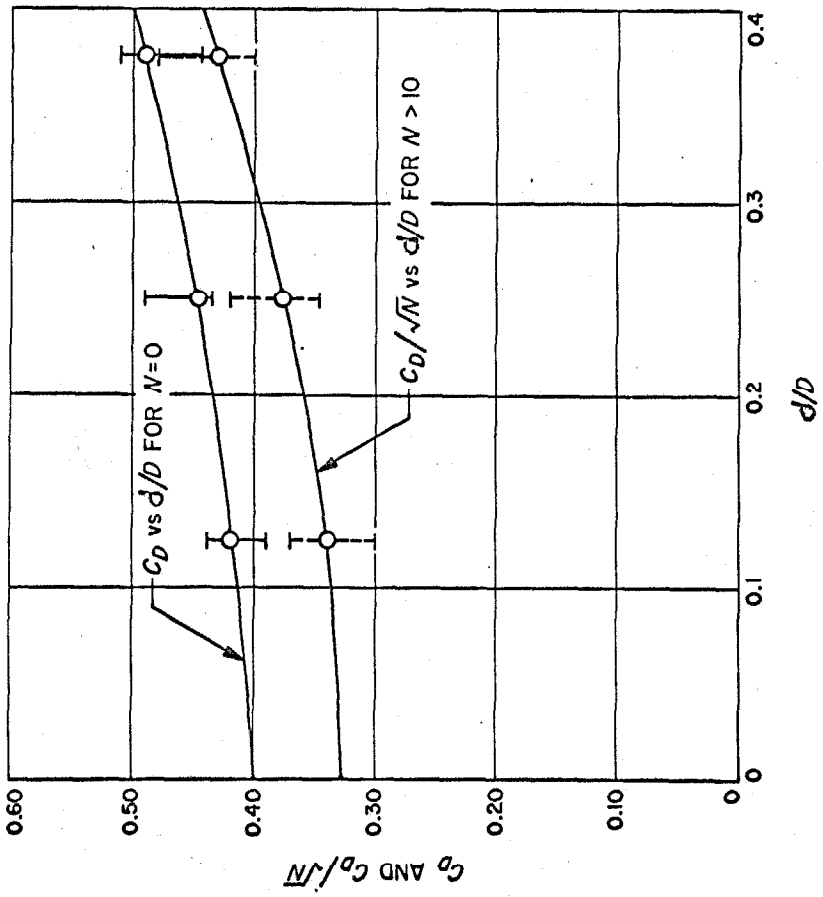

FIG. 17 Blockage Effect for Spheres

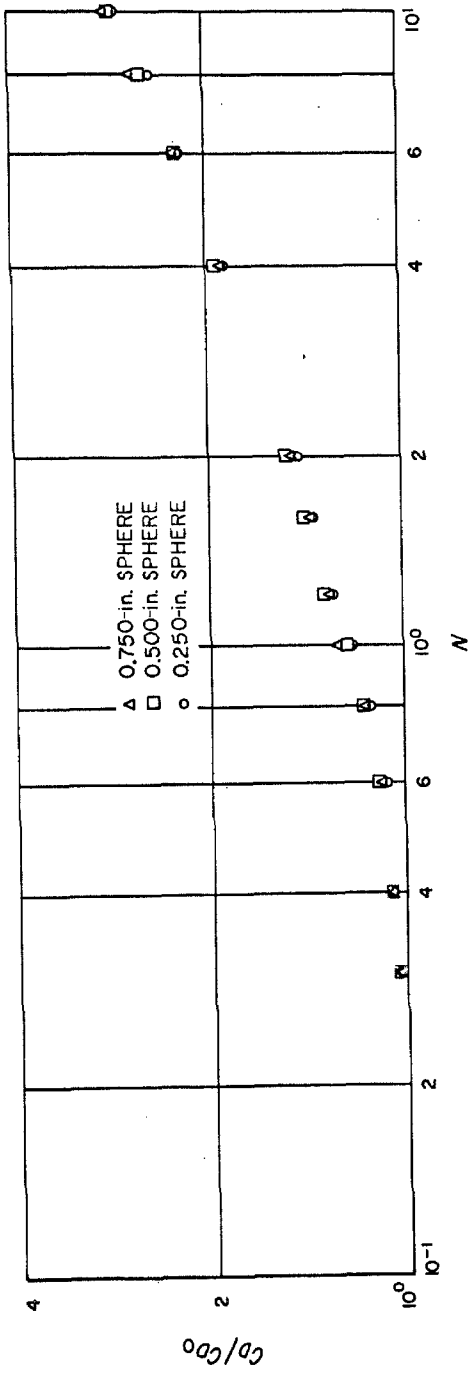

FIG. 18 C_D/C_{D_o} Vs Interaction Parameter for Spheres

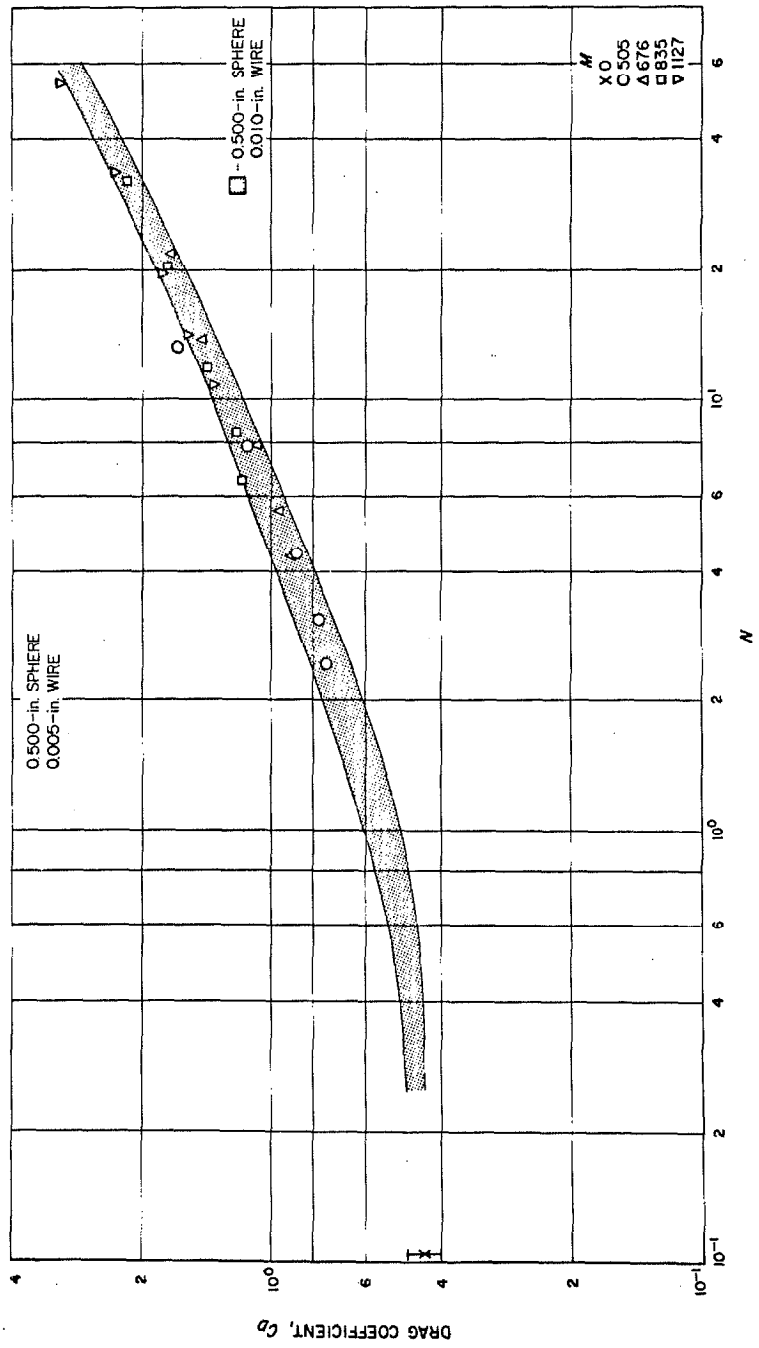

FIG. 19 Drag Coefficient Vs Interaction Parameter for 0.500-In. Sphere Showing Effect of Wire Size

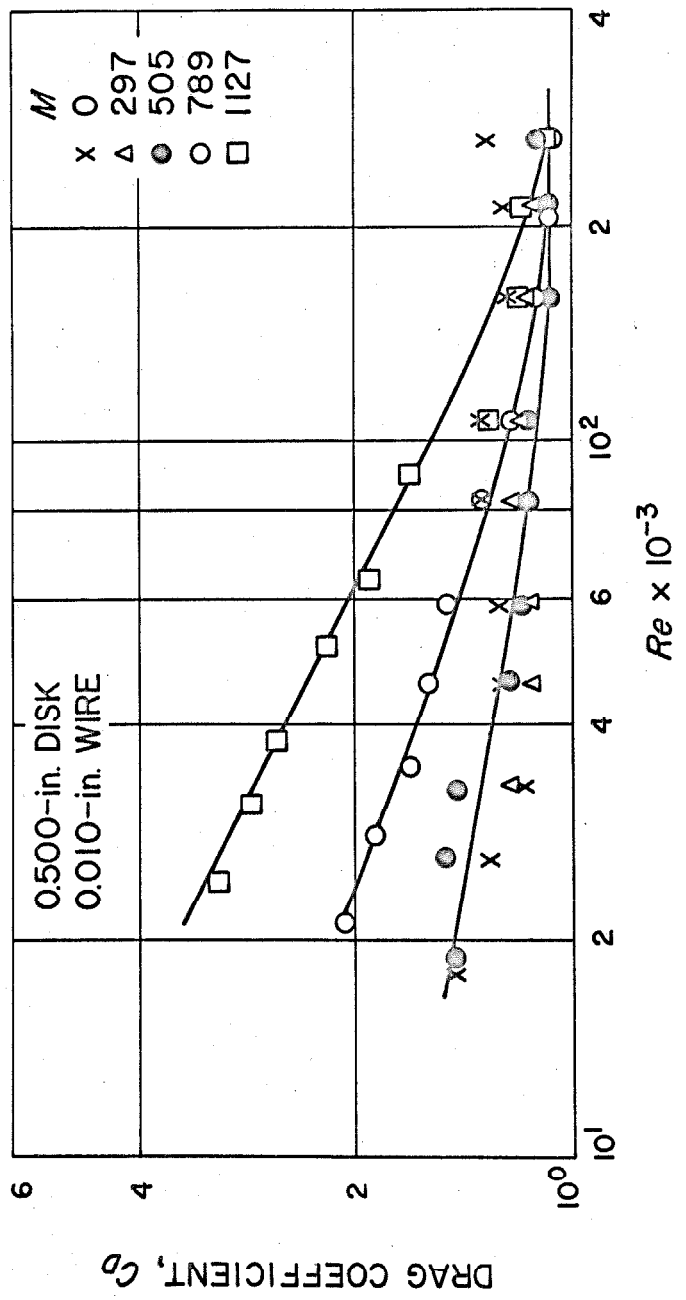

FIG. 20 Drag Coefficient Vs Reynolds Number for 0.500-In. Disk

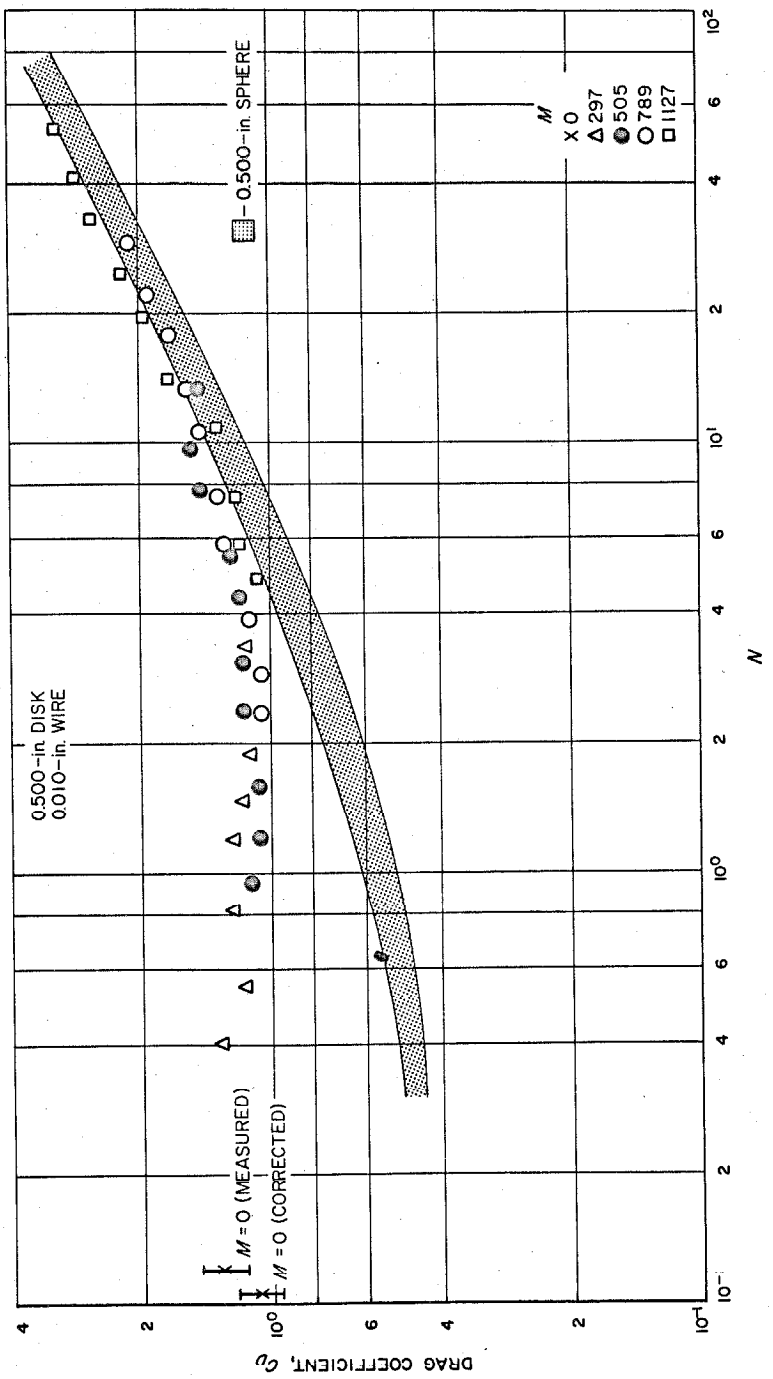

FIG. 21 Drag Coefficient Vs Interaction Parameter for 0.500-In. Disk

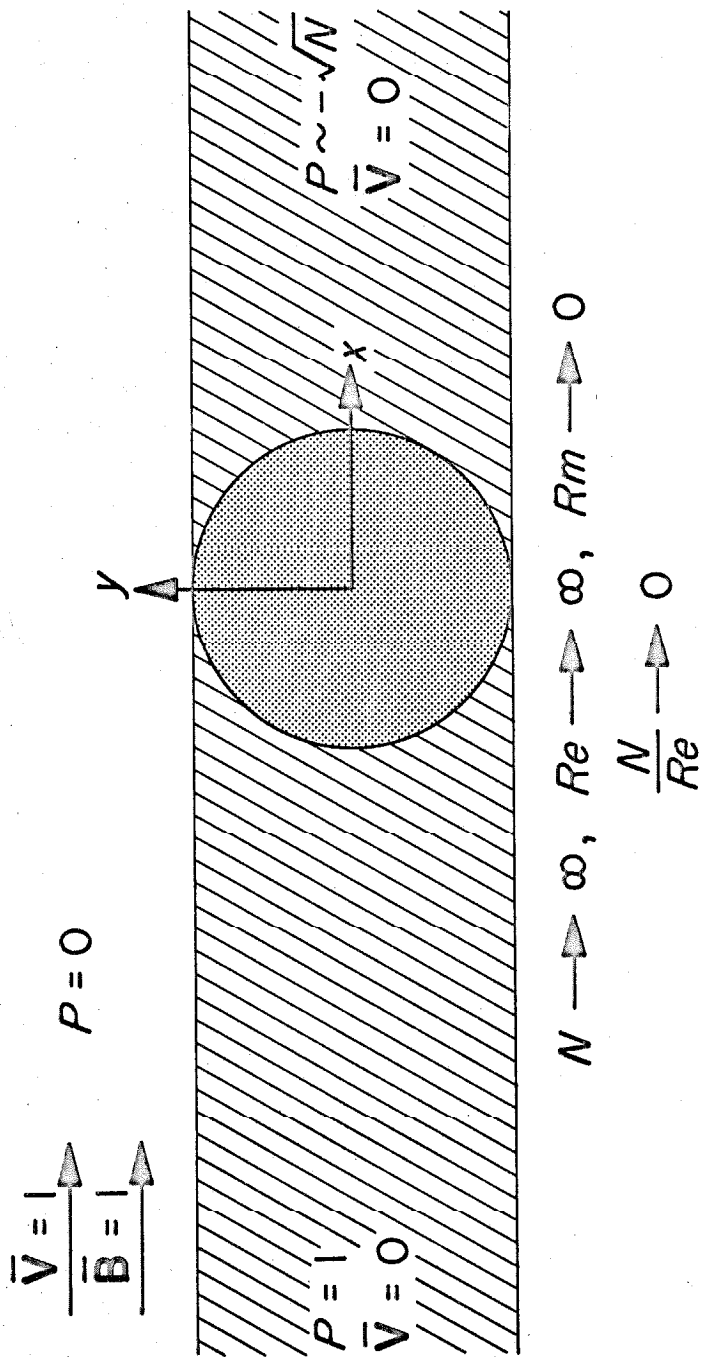

FIG. 22 Limiting Flow Field